AD_____

Award Number: W81XWH-06-1-0363

TITLE: The Role of Osteoblast-Derived Cytokines in Bone Metastatic Breast Cancer

PRINCIPAL INVESTIGATOR: Karen M. Bussard, B.S., M.S.

CONTRACTING ORGANIZATION: The Pennsylvania State University
University Park, PA 16802

REPORT DATE: March 2007

TYPE OF REPORT: Annual Summary

PREPARED FOR: U.S. Army Medical Research and Materiel Command
Fort Detrick, Maryland 21702-5012

REPORT DOCUMENTATION PAGE

Form Approved
OMB No. 0704-0188

1. REPORT DATE *(DD-MM-YYYY)*	**2. REPORT TYPE**	**3. DATES COVERED** *(From - To)*
01/03/07	Annual Summary	1 Mar 2006 – 28 Feb 2007

4. TITLE AND SUBTITLE

The Role of Osteoblast-Derived Cytokines in Bone Metastatic Breast Cancer

5a. CONTRACT NUMBER

5b. GRANT NUMBER
W81XWH-06-1-0363

5c. PROGRAM ELEMENT NUMBER

6. AUTHOR(S)
Karen M. Bussard, B.S., M.S.

E-Mail: kmb337@psu.edu

5d. PROJECT NUMBER

5e. TASK NUMBER

5f. WORK UNIT NUMBER

7. PERFORMING ORGANIZATION NAME(S) AND ADDRESS(ES)

The Pennsylvania State University
University Park, PA 16802

8. PERFORMING ORGANIZATION REPORT NUMBER

9. SPONSORING / MONITORING AGENCY NAME(S) AND ADDRESS(ES)
U.S. Army Medical Research and Materiel Command
Fort Detrick, Maryland 21702-5012

10. SPONSOR/MONITOR'S ACRONYM(S)

11. SPONSOR/MONITOR'S REPORT NUMBER(S)

12. DISTRIBUTION / AVAILABILITY STATEMENT
Approved for Public Release; Distribution Unlimited

13. SUPPLEMENTARY NOTES

14. ABSTRACT: Breast cancer (BC) metastasizes to bone. It is likely bone provides a hospitable environment that attracts BC cells and allows them to colonize and grow. Current models suggest BC-derived cytokines are key to understanding BC metastasis. We hypothesize that osteoblasts can be directed by metastatic BC cells to produce cytokines that are chemoattractants for osteoclasts and cancer cells, and growth or maintenance factors for BC cells. Our purpose is to determine how osteoblast-derived cytokines influence BC metastases to bone. Goals include investigating the production of osteoblast-derived cytokines in response to BC cells or their conditioned medium (CM), the production of bone-derived cytokines in response to BC cells in vivo, and the presence of functional cytokine receptors on osteoblasts and BC cells. Using murine osteoblasts, and human metastatic BC and non-metastatic cells, we found that BC CM treatment increased osteoblast-derived cytokine secretion of IL-6, KC, VEGF, MIP-2, and MCP-1. Maximum induction of osteoblast-derived cytokine secretion occurred with 20 day old cells. Treatment with CM of a bone-seeking cancer variant enhanced osteoblast-derived cytokine production at Day 20. Murine-specific ELISAs showed osteoblast-derived cytokine secretion to MDA-231 variant CM was dose-dependent. No significant changes in osteoblast-derived cytokine secretion were observed in 4 day old cells.

15. SUBJECT TERMS
osteoblast, metastasis, MDA-MB-231, IL-6, MCP-1, KC, MIP-2, VEGF

16. SECURITY CLASSIFICATION OF:			**17. LIMITATION OF ABSTRACT**	**18. NUMBER OF PAGES**	**19a. NAME OF RESPONSIBLE PERSON**
a. REPORT	**b. ABSTRACT**	**c. THIS PAGE**			USAMRMC
U	U	U	UU	42	**19b. TELEPHONE NUMBER** *(include area code)*

Table of Contents

	Page
Introduction……..	**1**
SF298……	**2**
Table of Contents……..	**3**
Body……..	**4-9**
Key Research Accomplishments……..	**9**
Reportable Outcomes……	**9-10**
Conclusion……	**10-11**
References……	**11-12**
Supporting Data……	**13-27**
Appendices……	**27 (- 42)**

INTRODUCTION

Breast cancer frequently metastasizes to bone[1]. Although the precise mechanism underlying preferential metastasis is unknown, it is likely that the bone provides a hospitable environment that both attracts breast cancer cells and allows them to colonize and grow[2]. Bone remodeling begins when bone resorbing osteoclasts excavate an erosion cavity in the matrix[3]. Following this, bone depositing osteoblasts migrate to the cavity and synthesize layers of osteoid matrix that mineralize and form new bone[3]. Metastatic breast cancer cells disrupt the tightly regulated balance between resorption and deposition, i.e. osteoclasts are constitutively activated, resulting in osteolytic lesions that cause bone pain and hypercalcemia[4]. Current therapies utilize bisphosphonates to block osteoclast function and slow osteolytic lesion progression[5]. Lesions already present, however, do not heal[6]. Osteoblasts do not synthesize new matrix and show altered properties including decreased proliferation, altered adhesion, and loss of differentiation[2, 7, 8]. It follows that metastatic breast cancer cells may affect osteoblasts as well as osteoclasts. Current models implicate chemokines and cytokines produced by breast cancer cells as keys to understanding breast cancer cell metastasis[9]. While they may play an important role, we have evidence that *osteoblasts* can be directed by metastatic breast cancer cells to produce inflammatory cytokines that may be chemoattractants, growth, or maintenance factors for the cancer cells or for osteoclasts. For my ongoing research, I hypothesize that ***osteoblast*-derived cytokines are increased in the presence of metastatic breast cancer cells and act as chemoattractants, growth, and maintenance factors for them.** The aims of this proposal are: 1) To determine how *osteoblast*-derived inflammatory cytokine production by MC3T3-E1 osteoblasts is altered in response to co-culture or conditioned media of bone metastatic MDA-MB-231 breast cancer cell variants. 2) To determine how bone-derived inflammatory cytokine production is altered in response to breast cancer cells *in vivo*. 3) To determine if osteoblasts and breast cancer cells have receptors and can respond to *osteoblast*-derived inflammatory cytokines.

BODY

Task 1. **To determine how *osteoblast*-derived inflammatory cytokine production by MC3T3-E1 osteoblasts is altered in response to co-culture or CM of bone metastatic MDA-MB-231 breast cancer cell variants. (Months 1-12)**

Task 1a (Months 1-2): Conditioned media (CM) was collected at 24 hours from the following cell lines: murine MC3T3-E1 osteoblasts (at 4 days, 10 days, and 20 days), hTERT-HME1 human mammary epithelial cells, human metastatic breast cancer cell lines MDA-MB-231W (parental population), MDA-MB-231PY (parental population identical to MDA-231W and used to develop MDA-231BO and MDA-231BR cells), bone-seeking MDA-MB-231BO, and brain-seeking MDA-MB-231BR, and human non-metastatic breast cancer cell line BRMS1 transfected-MDA-MB-231. Murine MC3T3-E1 conditioned medium was also collected at 12 hours. Conditioned media (CM) was obtained by growing cells to confluence and incubating them in serum-free media for 24 (or 12) hours. CM was stored at >-20°C until used.

Task 1b (Months 3-4): Species-specific ELISAs and a human Bio-Rad Bio-Plex™ were used to quantitate the amount of inflammatory cytokines present in the collected CM. IL-6 was used as an initial screening cytokine. Twelve-hour CM obtained from osteoblasts grown to either 4 or 10 days contained no (0 pg/ml) IL-6. Twelve-hour CM obtained from osteoblasts grown to 20 days has not yet been tested. Twenty-four hour CM obtained from osteoblasts grown to either 4 or 10 days contained no (0 pg/ml) IL-6. Twenty-four hour CM obtained from osteoblasts grown to 20 days contained an average of 18 pg/ml IL-6. From other experiments carried out in our laboratory, it was found that by 24 hours, the osteoblasts may be undergoing a stress response from treatment with serum-free media (α-MEM) that is used for the production of CM. This stress response from the serum free media may skew the "normal" cytokine production. Thus, we used CM obtained from osteoblasts at 12 hours in future experiments.

In a related study, cytokine expression in selected human metastatic breast cancer CM was quantitated using a human Bio-Rad Bio-Plex™. MCP-1 was notably absent or present in very low levels in all of the human lines examined. IL-6 and IL-8 were present in lower levels in MDA-231W CM, but expressed in larger concentrations in MDA-231BO and MDA-231BR CM (Figure 1). Further human cytokine arrays assaying for human cytokine secretion in CM and culture supernatants have not yet been carried out. A human Bio-Rad Bio-Plex™ has recently been purchased for this purpose and will be conducted in the upcoming weeks.

Three improvements to this task include: i) Alkaline phosphatase staining of differentiating MC3T3-E1 osteoblasts in vitro (indicating bone turnover) is typically evident by 9 days. Thus, it was suggested by my thesis committee to chose a time point more representative of early differentiation: 10 days as opposed to 14. Thus, murine osteoblasts were grown to 10 days instead of 14 in future experiments. ii) As evidenced by task 1c-d (see below), an unexpectedly large increase in osteoblast-derived cytokine production was seen when osteoblasts were treated with non-metastatic (hTERT-HME and MDA-231BRMS) cell CM. Thus, an additional non-metastatic cell line, MDA-MB-468, was added to experiments to verify the cytokine response. CM has been collected from this human non-metastatic cell line and will be quantified using a human Bio-Rad Bio-Plex™. In addition, iii) a further sample analysis will be carried out using a human Bio-Rad Bio-Plex™ and subsequently verified using standard ELISAs.

Task 1c-d (Months 5-8): MC3T3-E1 osteoblasts were grown to either 4, 10, or 20 days. Cells were stained for alkaline phosphatase expression (bone turnover) and von Kossa (mineralization) to verify their stage of differentiation (Figure 2). Alkaline phosphatase expression was evident by day 10 and mineralization was present by day 20 (Figure 2). These results are consistent with previous data obtained in our laboratory. Differentiation media was then replaced with either 0, 10, 25, or 50% CM from the cells listed in Task 1a-b. Twenty-four hours later, culture media was collected, centrifuged to remove any debris, and stored at >-20°C until use. This experiment was conducted in duplicate and repeated twice for a total of $n \geq 4$ samples collected per condition. Murine ELISAs were used to determine if osteoblast-derived cytokine response to the addition of MDA-231 variant CM was dose-dependent. It was found that osteoblast-derived cytokine secretion was for the most part dose-dependent at days 10 and 20 (Figure 3). No significant changes in osteoblast-derived cytokine secretion was seen on day 4 between the various CM treatments (compare Figure 4a-c). Significant changes,

including a clear dose- and heightened response, were seen at days 10 and 20 (Figure 4b and c). As a result, it was decided that Day 4 (growth) would be ruled out of further study. From this point on, osteoblasts will only be grown to 10 (early differentiation) or 20 (late differentiation) days for use in this investigation.

Next, a Bio-Rad Bio-Plex™ 32 x-Plex Murine Cytokine Assay was used to quantitate the MC3T3-E1 osteoblast-derived cytokine response to 50% MDA-231 variant CM. The Bio-Rad Bio-Plex™ 32 x-Plex Murine Cytokine Assay consisted of the following cytokines:

- IL-1α
- IL-1β
- IL-2
- IL-3
- IL-4
- IL-5
- IL-6
- IL-9
- IL-10
- IL-12 p40
- IL-12 p70
- IL-13
- IL-17
- Eotaxin
- G-CSF
- GM-CSF
- IFN-γ
- KC
- MCP-1
- MIP-1α
- MIP-1β
- RANTES
- TNF-α
- IL-15
- IL-18
- FGF-basic
- LIF
- M-CSF
- MIG
- MIP-2
- PDGF-BB
- VEGF

The osteoblast response to CM from metastatic and non-metastatic cells was then assessed.

Surprisingly, at 10 days old, the largest response in osteoblast-derived cytokine secretion was seen with the addition of CM from a brain-seeking variant (Figure 5a, orange slashed bar). At 20 days old, however, this response was seen with the addition of CM from a bone-seeking variant (Figure 5b, blue checked bar). Maximum induction of osteoblast-derived cytokine response can be seen in more differentiated (20 day old) cells. This suggests that osteoblast age (differentiation stage) is an important factor in examining the cytokine response to breast cancer cell treatments.

Quite surprisingly, there was a very large osteoblast-derived cytokine response to the addition of both types of non-metastatic cell CM (Figure 6). This effect was repeatedly seen. The osteoblast-derived cytokine response to non-metastatic cell CM was, for the most part, greater than that seen with the addition of metastatic CM (compare Figure 5 with Figure 6). Intriguingly, there was no osteoblast-derived cytokine production of MCP-1 at day 10 with the addition of either non-metastatic CM (Figure 6a) or with osteoblast treatment of hTERT-HME1 CM at day 20 (Figure 6b). A large osteoblast-derived MCP-1 response was seen with the addition of metastatic cell CM at day 10 (Figure 5a) and was more collectively seen at day 20 (Figure 5b). Recall that MCP-1 was a cytokine that was either absent or present in very low amounts in human metastatic breast cancer CM (Figure 1). Thus, MCP-1 has been identified as a cytokine of extreme interest in breast cancer metastasis to bone.

As a result of the unexpectedly large increase in cytokine production that was seen when osteoblasts were treated with non-metastatic (hTERT-HME and MDA-

231BRMS) cell CM, an additional non-metastatic cell line, MDA-MB-468, was added to experiments to compare the cytokine response. MC3T3-E1 osteoblasts were grown to either 10 or 20 days. Differentiation media was replaced with either 0, 10, 25, or 50% MDA-MB-468 CM. Twenty-four hours later, culture media was collected, centrifuged to remove any debris, and stored at >-20°C until use. At the present, samples for this experiment have been collected and repeated at the 20 day time point (for a total of n=4 samples per condition), and have been collected for the 10 day time point (for a total of n=2 samples per condition). This experiment is currently being repeated (for a total of n=4 samples per condition) for the 10 day time point. A Bio-Rad Bio-Plex™ Murine Cytokine array will be used to quantitate the MC3T3-E1 osteoblast-derived cytokine response.

Task 1e-f (Months 9-12): Preliminary experiments were carried out in order to 1) examine differences in using 0.4 μm pore size transwell plate inserts and 3 μm pore size transwell plate inserts; 2) to determine if MDA-MB-231W cells affect MC3T3-E1 osteoblasts differently than MDA-MB-231GFP cells; and 3) to determine if osteoblasts and breast cancer cells grown in a transwell system yield different results than CM treatment or direct co-culture. MC3T3-E1 osteoblasts were grown to 11 days in 24 well plates. On day 10, MDA-231W or MDA-231GFP cells were plated (at a density recommended by the manufacturer) in either 0.4 μm pore size inserts or 3 μm pore size inserts. Human metastatic breast cancer cells were allowed to adhere overnight. Twenty-four hours later, all media was removed from wells and inserts, cells were rinsed with PBS, and media replaced with fresh differentiation media. Breast cancer cell inserts were transferred to wells containing 10 or 20 day old osteoblasts. The cell culture system was incubated for an additional four days at which point culture media was collected, centrifuged to remove any debris, and stored at >-20°C until use. This experiment was conducted in triplicate (n=3 samples per condition). A variety of assays were carried out: 1) Alkaline phosphatase enzyme activity was assessed using an alkaline phosphatase enzyme kit. While results were not consistent, a few trends can be seen (Table 1). Overall, murine osteoblasts grown in transwell dishes with 0.4 μm pore size produced more alkaline phosphatase activity. Lower amounts of alkaline phosphatase were present in cells grown in transwell plates with 3 μm pore size. Light and fluorescent microscope pictures were then taken of: a) the plate and inserts together, b) the plate (MC3T3-E1 osteoblasts) by themselves, and c) the insert (MDA-MB-231GFP cells) by themselves. It was seen by fluorescence microscopy that although some human breast cancer cells migrated through the pores to the underside of the insert (Figure 7b), none migrated into the MC3T3-E1 osteoblast layer (Figure 7a). Thus, the four day incubation period between the time that the breast cancer cells were plated and the time that culture supernatants were obtained was adequate for further experimentation. Finally, a murine IL-6 ELISA was conducted on the culture supernatants obtained from the experiment. The largest murine osteoblast-derived IL-6 response was seen in the 3 μm pore size system (Figure 8). The IL-6 response elicited by the murine osteoblasts in the 0.4 μm pore size system was either absent or greatly reduced (Figure 8). Finally, there was a ~10 pg/ml difference between the effect of MDA-231W and MDA-231GFP cells on osteoblast-derived IL-6 response in the 3 μm pore size system (Figure 8). These differences were considered minimal. Based on these results, we chose transwell inserts with a 3 μm pore size for future experiments.

MC3T3-E1 murine osteoblasts were grown to either 10 or 20 days in 24 well plates. At day 9 or 19 of osteoblast differentiation, MDA-231 human metastatic cell variants (MDA-231W, MDA-231PY, MDA-231BO, and MDA-231BR) were plated in separate plates at the following ratios of osteoblast : non-osteoblast: "1:2," "1:1," and "10:1." The ratios of osteoblast : non-osteoblast were based on related experiments conducted in the laboratory. Breast cancer cells were allowed to adhere overnight. On day 10 or 20, all media was removed from wells and inserts, cells were rinsed with PBS, and media replaced with fresh differentiation media. Breast cancer cell inserts were transferred to wells containing 10 or 20 day old osteoblasts. The cell culture system was incubated for an additional three days at which point culture media were collected, centrifuged to remove any debris, and stored at >-20°C until use. This experiment has presently been carried out one time in duplicate (n=2 samples per condition). A repeat experiment (for a total of n≥4 samples collected per condition) is currently underway. Once all samples have been collected, they will be assayed for the presence of osteoblast-derived cytokine secretion using a Bio-Rad Bio-Plex™ Murine Cytokine array. This experiment will also be repeated for a total of n≥4 samples collected per condition using MDA-231BRMS, MDA-MB-468, and hTERT-HME1 cells.

Task 2. **To determine how bone-derived inflammatory cytokine production is altered in response to breast cancer cells *in vivo*. (Months 13-17)**

In a pilot study, we found that osteoblasts in the bone naturally produce cytokines that may be chemoattractants for metastatic breast cancer cells. In order to carry out the study, I learned how to perform intracardiac inoculations of athymic nude mice. Femurs from either control or mice inoculated via intracardiac injection with metastatic breast cancer cells were assayed *ex vivo* for inflammatory cytokines using species-specific antibody arrays. In particular, we showed that metaphyses (ends) of bone in normal mice cleared of bone marrow produced substantial amounts of KC, MIP-2, IL-6, and MCP-1. In mice inoculated with the MDA-231 variant, metastatic breast cancer cells predominantly trafficked to the metaphyses of the bone[11], where concentrations of MCP-1, IL-6, MIP-2, and KC increased from control values significantly (Figure 9). In addition, a Bio-Rad Bio-Plex™ 32 x-Plex Murine Cytokine Assay (see above for cytokine listing) was used to quantitate murine cytokine production. In Figure 10 and 11, it can be seen that, based on the treatment [A) control, B) MDA-MB-231-GFP inoculated, or C) MDA-MB-435-GFP inoculated], cytokines and their concentrations varied between bone ends and shaft. While these data are still being analyzed, it can be noted that larger amounts of osteoblast-derived IL-6, KC, MCP-1, and MIP-2 (murine homologue to human IL-8; homology with KC) are generally found in the ends of long bones as compared to the shaft, which is to where bone metastatic breast cancer cells initially traffick[11] (see the following discussion). Thus, preliminary results implicate these cytokines as important factors in the metastasis of breast cancer to bone.

Additionally, a novel experiment was conducted that monitored and quantified breast cancer cell trafficking in the bone. The DNA from femurs of mice inoculated with MDA-231GFP cells were isolated at various times, purified, and subjected to quantitative PCR for a human gene, HERV-1. Then the number of breast cancer cells was calculated. Femurs were separated into metaphyses and diaphyses. Results indicated that breast cancer cells preferentially migrated within days directly to the distal then proximal

metaphyses. Few were found in the diaphyses[11] (and appendix). Taken together, these results suggest that metastatic cancer cells are attracted to cytokines naturally secreted by osteoblasts.

Task 3. **To determine if osteoblasts and breast cancer cells have receptors and can respond to *osteoblast*-derived inflammatory cytokines. (Months 18-33)**

Task 3 has not yet been addressed.

Task 4. **Final data analysis and thesis preparation. (Months 34-36)**

Task 4 has not yet been carried out.

Progress in Program: From the time this proposal was submitted, all required course work for a Ph.D. has been completed. In December 2005, I passed my candidacy examination; and in June 2006, I successfully completed my comprehensive examination.

KEY RESEARCH ACCOMPLISHMENTS

- It was discovered that osteoblasts are an important source of KC, MCP-1, IL-6, MIP-2, and VEGF in the vicious cycle of breast cancer bone metastasis. MCP-1 is a particular cytokine of interest in this group because it was not expressed by breast cancer cell CM or osteoblasts treated with non-metastatic cell CM.
- Osteoblast-derived cytokine production in response to MDA-231 variant CM was found to be dose-dependent.
- Maximum induction of osteoblast-derived cytokine secretion was found to occur in more differentiated (20 day old) cells. This suggests that the stage of osteoblast differentiation is important in determining the osteoblast response to metastatic breast cancer cells.
- It was discovered that treatment with the CM of a MDA-231 bone seeking variant further enhanced osteoblast-derived cytokine production at day 20.
- Finally, data suggest that osteoblast-derived cytokine production is necessary, but not sufficient, for the survival of bone metastatic breast cancer.

REPORTABLE OUTCOMES

Publications:

2007 Kinder, M, Chislock, EM, **Bussard, KM**, Shuman, LA, Mastro, AM. Metastatic Breast Cancer Induces an Osteoblast Inflammatory Response. Submitted.

2006 Phadke, PA, Mercer, RR, Harms JF, Jia, Y, Kappes, JC, Frost, AR, Jewell, JL, **Bussard, KM,** Nelson, S, Moore, C, Gay, CV, Mastro, AM, Welch, DR. "Kinetics of Metastatic Breast Cancer Cell Trafficking in Bone." Clinical Cancer Research. 12: (5) 1431.

Oral Presentations:

2006 **Bussard, KM,** Phadke, PA, Mercer, RR, Harms JF, Jia, Y, Kappes, JC, Frost, AR, Jewell, JL, Nelson, S, Moore, C, Gay, CV, Mastro, AM, Welch, DR. "Kinetics of Metastatic Breast Cancer Cell Trafficking in Bone." Presented at the American Association for Cancer Research Annual Meeting's Tumor Biology Minisymposium, April 1-5, 2006.

Abstracts / Poster Presentations:

2007 **Bussard, KM**, Mastro, AM. "Osteoblast-derived Inflammatory Cytokines are Produced in Response to Human Metastatic Breast Cancer Cells." The 100th Annual American Association for Cancer Research Annual Meeting, Los Angeles, CA, April 14-18, 2007. Proceedings of the 97th Annual Meeting for American Association for Cancer Research.

2006 **Bussard, KM,** Chislock, EM, Kinder, M, Gay, CV, Mastro, AM. "A Classic Set of Osteoblast-Derived Inflammatory Cytokines is Produced in Response to Bone Metastatic Breast Cancer." The 11th International Congress of the Metastasis Research Society, Tokushima, Japan, September 3-6, 2006 .

2005 **Bussard, KM,** Shuman, LS, Mercer, RR, Phadke, PA, Nelson, SM, Jewell, JL, Chislock, EM, Kinder, M, Welch, DR, Gay, CV, Mastro, AM. "The Interaction of Metastatic Breast Cancer Cells with Osteoblasts." Presented at the CrossOver 2005 Meeting sponsored by The Huck Institutes of The Life Sciences and The Materials Research Institute, The Pennsylvania State University, October 13-14, 2005.

Research Opportunities Applied for Based on this Research:

2006, 2007 The Edward A. Smuckler Memorial Workshop held through the American Association for Cancer Research (applied in 2006 but not admitted. Admitted in 2007.)

Awards / Grants / Fellowships Won Based on this Research:

2006 American Association for Cancer Research – Women in Cancer Research Brigid G. Leventhal Scholar Award in Cancer Research

2005-2006 Sigma Xi Grants-in-Aid of Research

2005-2007 The Pennsylvania Space Grant Consortium NASA Space Grant Fellowship

CONCLUSION

Alterations in the bone microenvironmet are extremely important in facilitating bone metastatic breast cancer. From these data, we believe that the following occurs: a) osteoblasts naturally secrete selected cytokines (IL-6, MCP-1, KC, MIP-2, and VEGF) at

low levels. These may serve as chemoattractants for breast cancer cells (invasion assays to further determine this have not yet been carried out) or may serve to prime the bone microenvironment for metastatic invasion. B) When a non-metastatic foreign cell enters the bone microenvironment, the osteoblast undergoes an inflammatory stress response and releases very large amounts of selected cytokines (IL-6, KC, and VEGF; a "normal" inflammatory response). C) However, when metastatic breast cancer cells invade the bone microenvironment, the osteoblasts secrete larger amounts of cytokines (IL-6, KC, and VEGF) than in a, but less than that seen in b. MCP-1, however, is secreted in significantly large amounts suggesting that this CC chemokine is a very important factor in breast cancer metastasis to bone. We also believe that the bone microenvironment is altered during this shift in cytokine expression and secretion (compare a to c) to favor breast cancer cell growth and development rather than that of chemoattraction. This hypothesis can be visually seen in a summary panel (Figure 12). Thus, comprehensive treatment of bone metastases must consider all cells present in the microenvironment in order to restore bone matrix deposition and limit osteolysis.

In summary, we propose that **metastatic breast cancer cells are attracted to inflammatory cytokines naturally produced by osteoblasts. Once in the bone microenvironment, the metastatic breast cancer cells induce the osteoblasts to undergo a stress response, increasing osteoblast production of inflammatory cytokines.**

REFERENCES

1. Roodman, GD. "Mechanisms of bone metastasis." N Engl J Med. 350: 2004. 1655-1664.
2. Mastro, AM, CV Gay, DR Welch. "The skeleton as a unique environment for breast cancer cells." Clin & Exp Metas. 20: 2003. 275-284.
3. Kanis, JA, EV McCloskey. "Bone turnover and biochemical markers in malignancy." Cancer. 80: 1997. 1538-1545.
4. Mundy, GR. "Metastasis to bone: causes, consequences and therapeutic opportunities." Nat Rev Cancer. 2: 2002. 584-593.
5. Hiraga, T, PJ Williams, GR Mundy. "The bisphosphonate ibandronate promotes apoptosis in MDA-MB-231 human breast cancer cells in bone metastases." Cancer Res. 61: 2001. 4418-4424.
6. Taube, T, I Elomaa, C Blomqvist, NC Benton, JA Kanis. "Histomorphometric evidence for osteoclast-mediated bone resorption in metastatic breast cancer." Bone. 15: 1994. 161-166.
7. Mastro, AM, CV Gay, DR Welch, HJ Donahue, J Jewell, R Mercer, D DiGirolamo, EM Chislock, K Guttridge. "Breast cancer cells induce osteoblast apoptosis: a possible contributor to bone degradation." J Cell Biochem. 91: 2004. 265-276.
8. Mercer, R, C Miyasaka, AM Mastro. "Metastatic breast cancer cells suppress osteoblast adhesion and differentiation." Clin & Exp Metas. 21(5): 2004. 427-435.
9. Guise, TA. "Molecular mechanisms of osteolytic bone metastases." Cancer. 88: 2000. 2892-2898.
10. Mercer, R, C Miyasaka, AM Mastro. "Metastatic breast cancer cells suppress osteoblast adhesion and differentiation." Clin & Exp Metas. 21: 2004. 427-435.

11. Phadke, PA, RR Mercer, JF Harms, J Yujiang, AR Frost, JL Jewell, KM Bussard, S Nelson, C Moore, JC Kappes, CV Gay, AM Mastro, DR Welch. "Kinetics of metastatic breast cancer cell trafficking in bone." Clin Cancer Res. 12: 2006. 1431-1440.

SUPPORTING DATA

Figure 1.: Human cytokine concentration in conditioned medium from selected MDA-MB-231 human metastatic breast cancer cell variants.

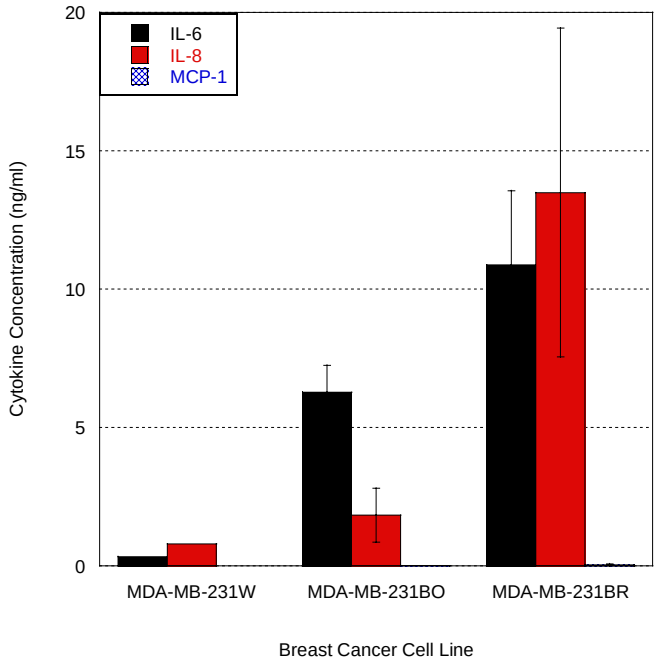

Conditioned media was prepared by growing cells to confluence. Growth medium was removed and cells were rinsed with PBS. Serum-free media (α-MEM, the base medium for MC3T3-E1 osteoblasts) was added to the breast cancer cells and was incubated for 24 hours. Conditioned medium was collected, centrifuged to remove any debris, and stored at >-20°C until used. Cytokines in the medium were quantified using human Bio-Rad BioPlex™ cytokine quantification assays.

Figure 2.: Alkaline Phosphatase Expression and von Kossa Staining of MC3T3-E1 Osteoblasts.

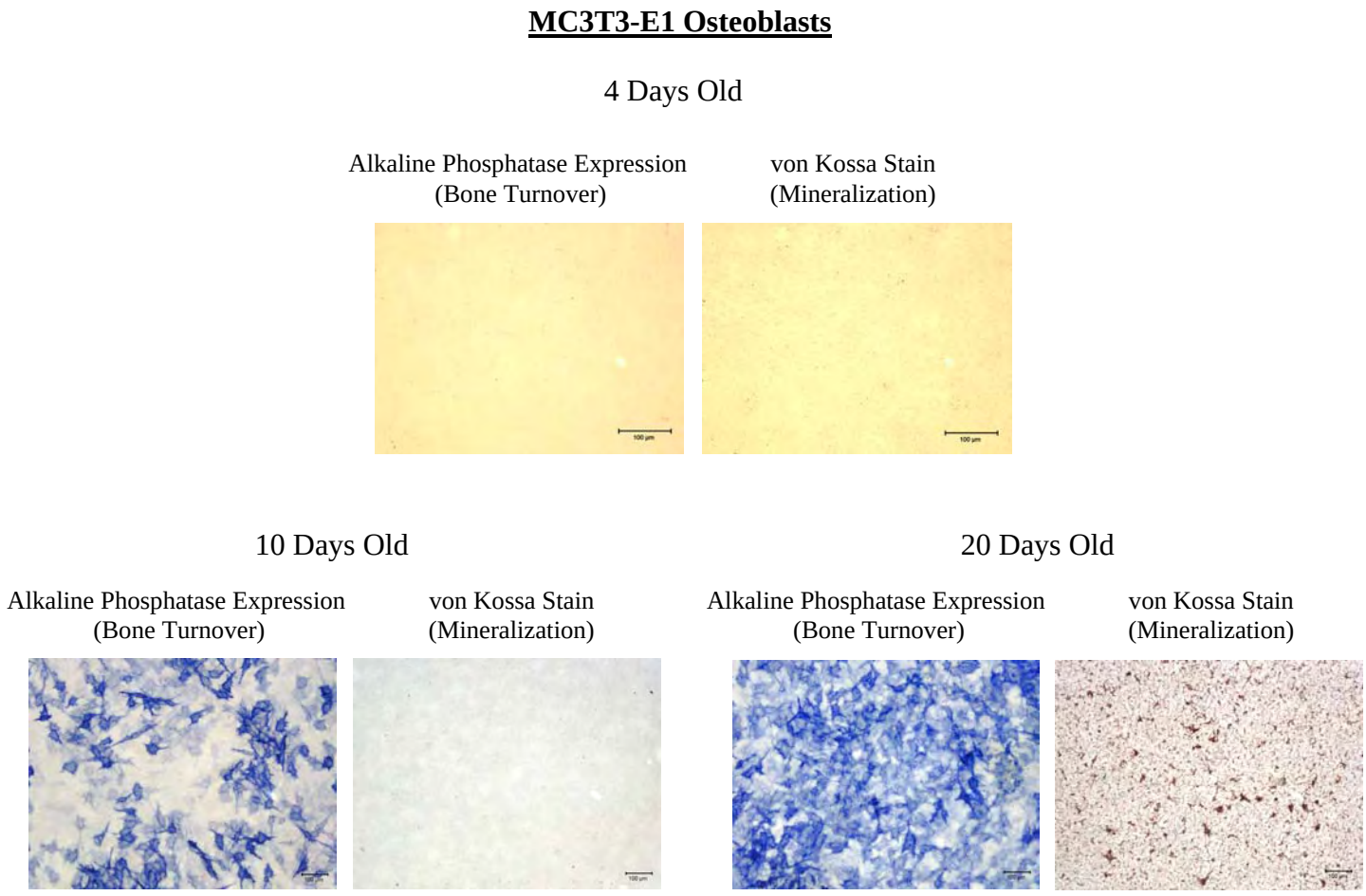

MC3T3-E1 osteoblasts were grown to either 4, 10, or 20 days. Cells were stained for alkaline phosphatase expression (bone turnover) and von Kossa (mineralization) to verify their stage of differentiation.

Figure 3.: Murine MC3T3-E1 cytokine response to treatment with various concentrations of conditioned medium from MDA-231 human metastatic breast cancer cells.

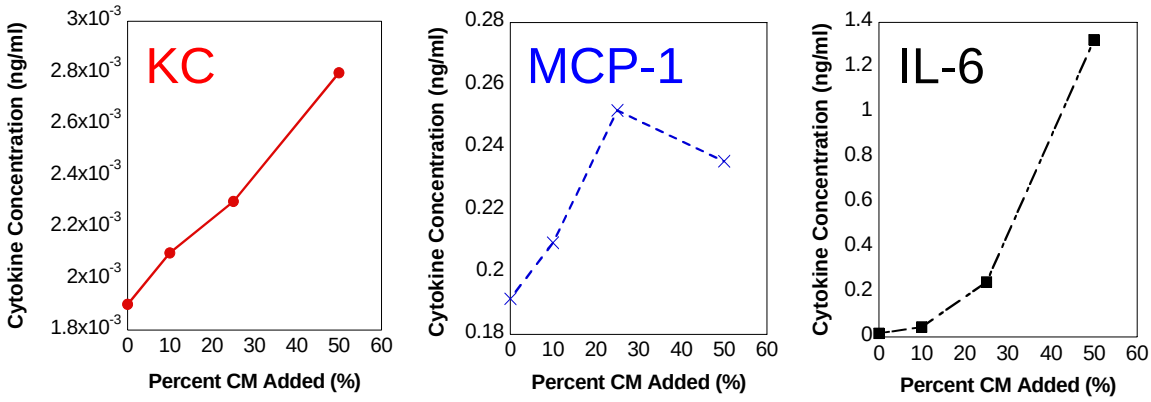

Murine MC3T3-E1 osteoblasts were grown to 4, 10, or 20 days. Osteoblasts were treated with 0, 10, 25, or 50% conditioned medium from MDA-231 cells for 24 hours. Murine cytokines in the medium were quantified using ELISAs. Shown is the cytokine response by murine osteoblasts, grown to 20 days, and treated with MDA-231PY conditioned medium.

Figure 4.: Comparison of MC3T3-E1 IL-6 response to treatment with conditioned medium from various human metastatic breast cancer cell lines.

A. MC3T3-E1 Osteoblasts Grown to 4 Days.

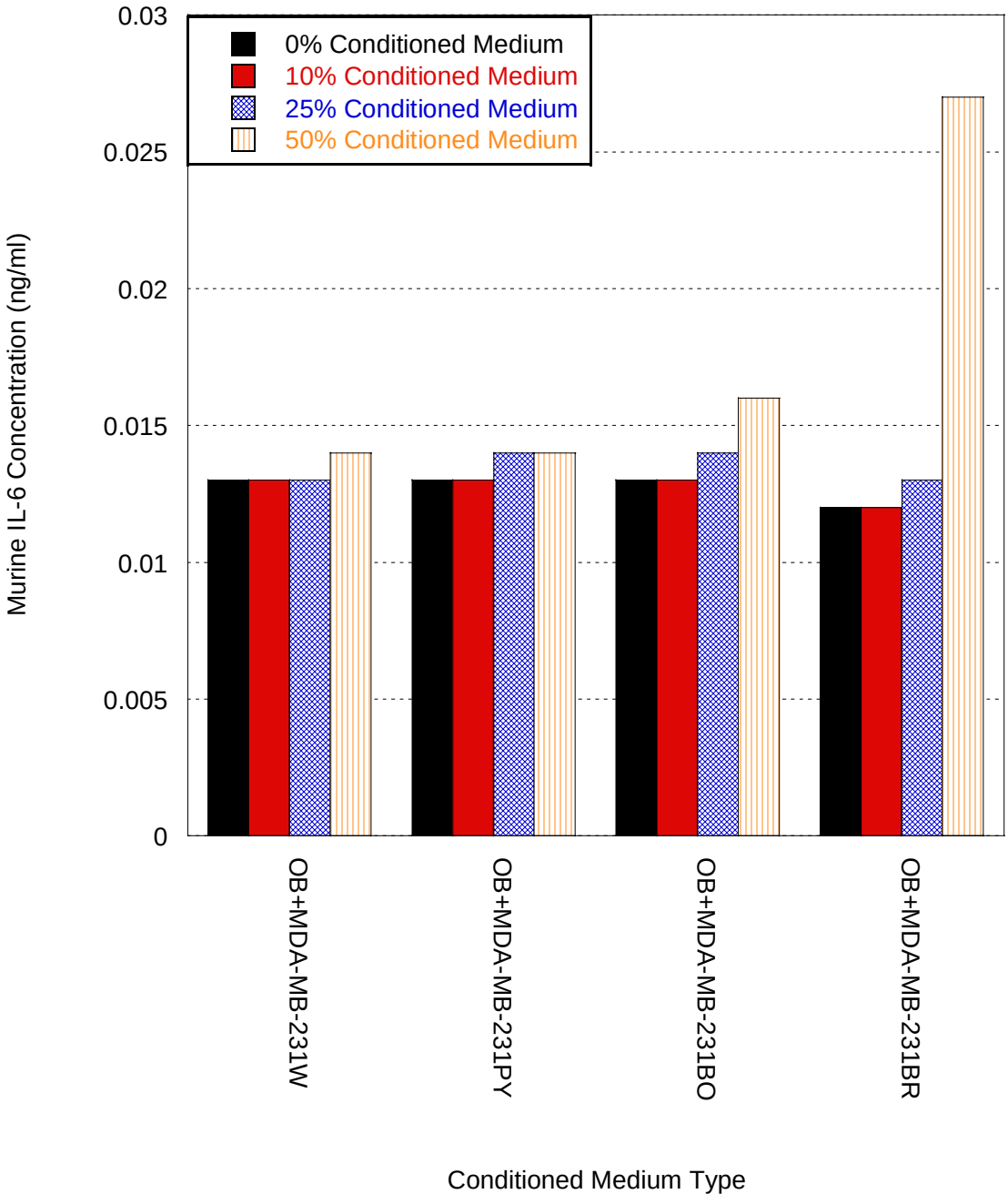

B. MC3T3-E1 Osteoblasts Grown to 10 Days.

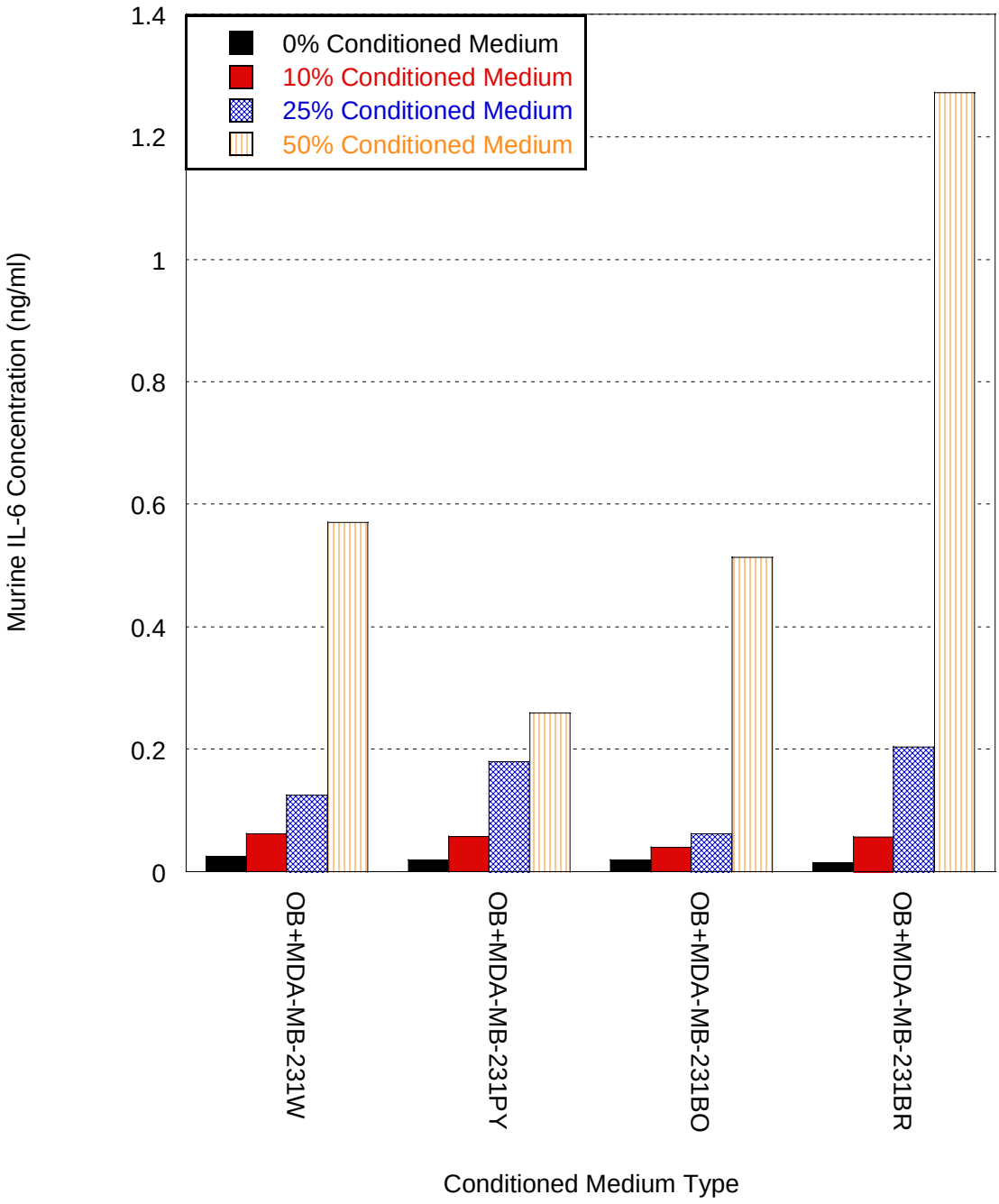

C. MC3T3-E1 Osteoblasts Grown to 20 Days.

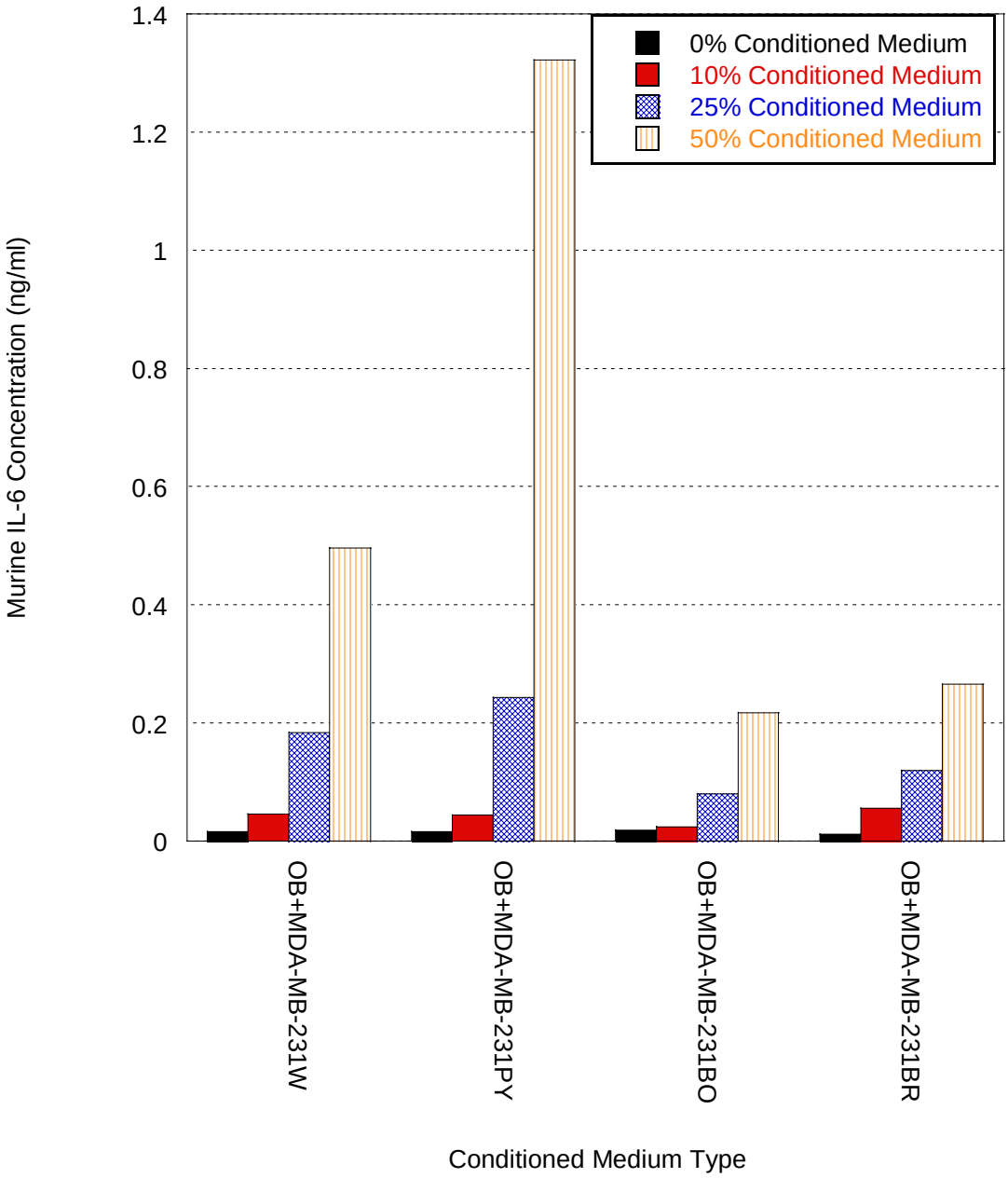

Murine MC3T3-E1 osteoblasts were grown to A) 4, B) 10, or C) 20 days. Osteoblasts were then treated with 0, 10, 25, or 50% conditioned medium from MDA-231 cells for 24 hours. Murine cytokines in the medium were quantified using ELISAs. Shown are representative experiments assaying for murine IL-6 concentration.

Figure 5.: Cytokine expression of MC3T3-E1 osteoblasts treated with 0 (VM) or 50% conditioned medium from MDA-231 cells.

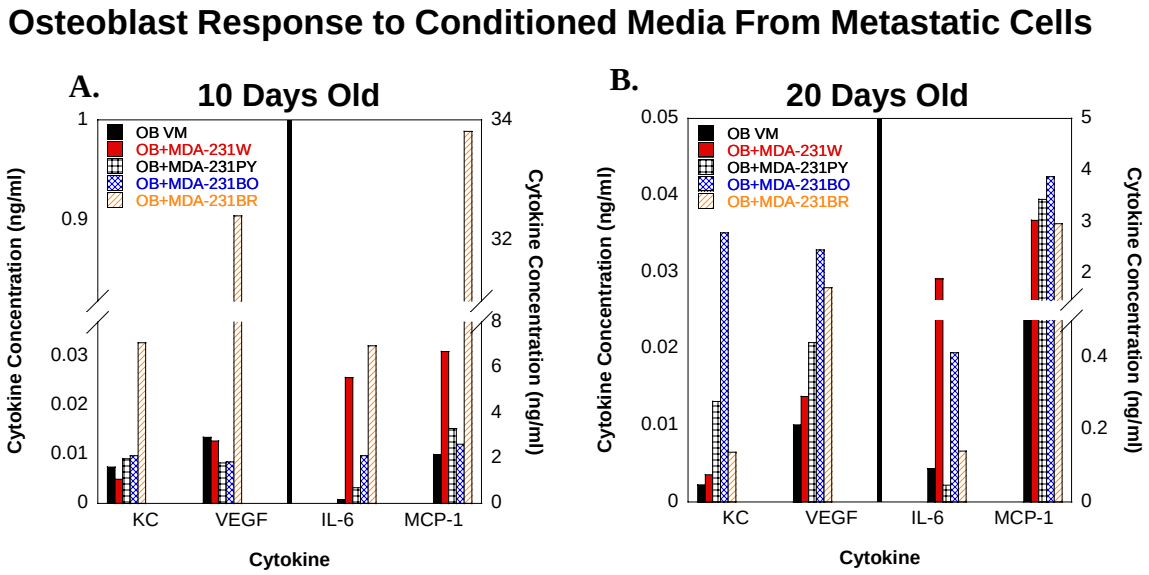

Murine MC3T3-E1 osteoblasts (grown to A) 10 or B) 20 days) were incubated with 0 or 50% conditioned medium from MDA-231 breast cancer cells for 24 hrs. Cytokines in the medium were quantified using Bio-Rad Bio-Plex™ Murine Cytokine quantification array.

Figure 6.: Cytokine expression of MC3T3-E1 osteoblasts treated with 0 (VM) or 50% non-metastatic cell CM.

Osteoblast Response to Conditioned Media From Non-Metastatic Cells

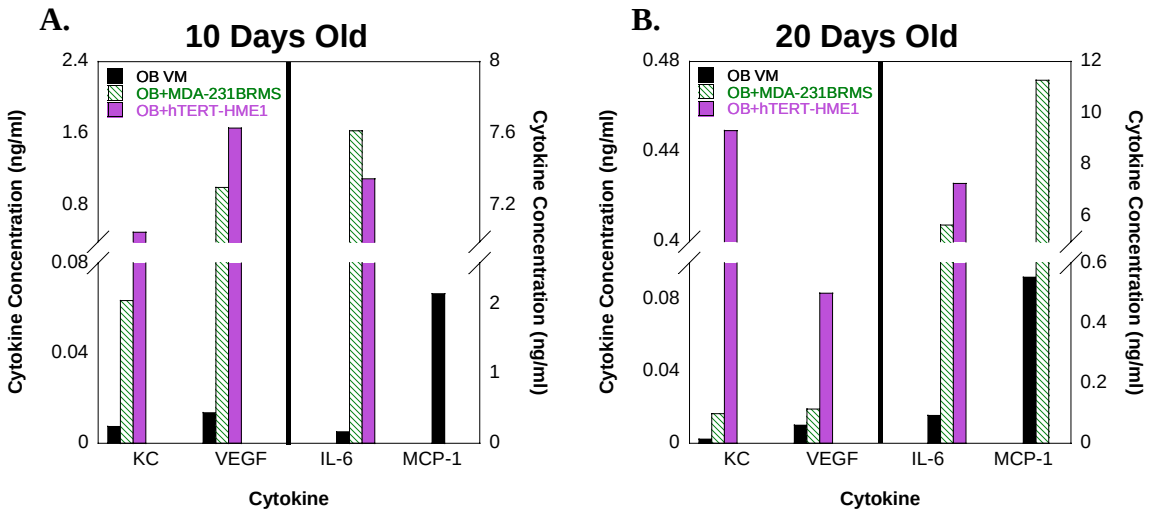

Murine MC3T3-E1 osteoblasts (grown to A) 10 or B) 20 days) were incubated with 0 or 50% non-metastatic cancer cell MDA-231BRMS or human mammary epithelial cell hTERT-HME1 CM for 24 hrs. Cytokines in the medium were quantified using Bio-Rad Bio-Plex™ Murine Cytokine quantification array.

Figure 7.: Light and fluorescent microscope images of 11 day old MC3T3-E1 murine osteoblasts in a transwell system with MDA-231W or MDA-231GFP human metastatic breast cancer cells.

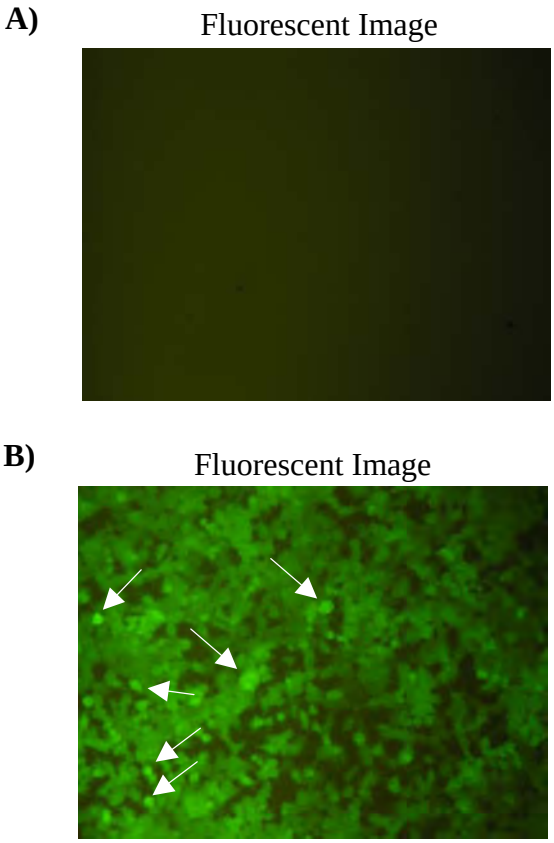

Light and fluorescent microscope images were taken of 11 day old MC3T3-E1 murine osteoblasts in a transwell system with either MDA-231W or MDA-231GFP human metastatic breast cancer cells. A) MC3T3-E1 murine osteoblasts in a fluorescent image that were plated in the bottom of a 24 well plate. B) Transwell plate insert containing MDA-MB-231GFP human metastatic breast cancer cells. These images were taken on an inverted microscope (i.e. looking from the bottom up through the plate and insert). GFP modified breast cancer cells that have migrated through the pores are clearly visible in the fluorescent image in B.

Figure 8.: Average MC3T3-E1 IL-6 response to incubation in a transwell system with human metastatic breast cancer cells.

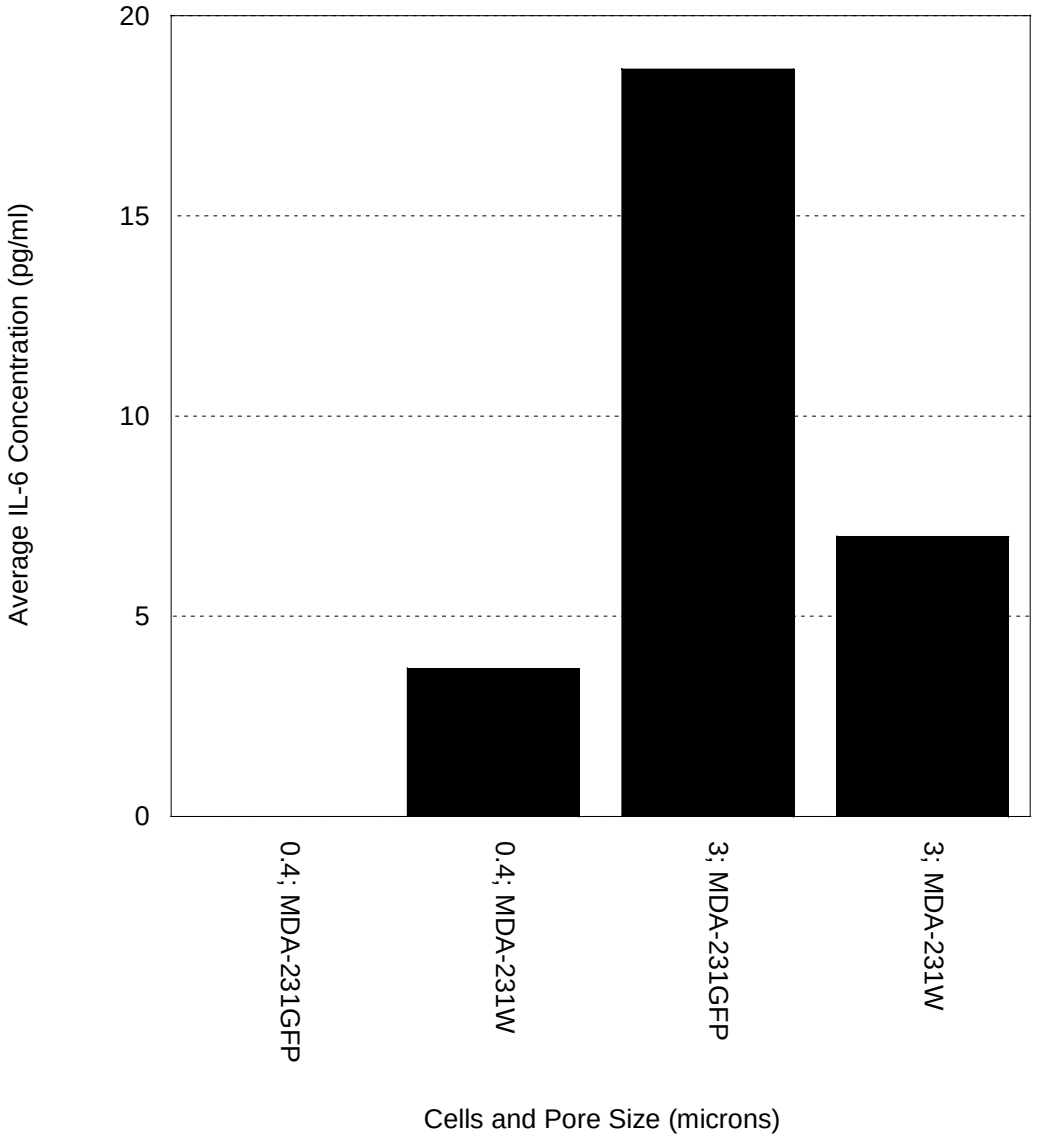

MC3T3-E1 murine osteoblasts grown to 11 days were incubated in a transwell system with either MDA-231W or MDA-231GFP human metastatic breast cancer cells for an additional 4 days. Osteoblast-derived IL-6 concentration was quantified using standard ELISAs.

Figure 9.: Cytokine expression of murine femur metaphyses ex-vivo following intracardiac inoculation.

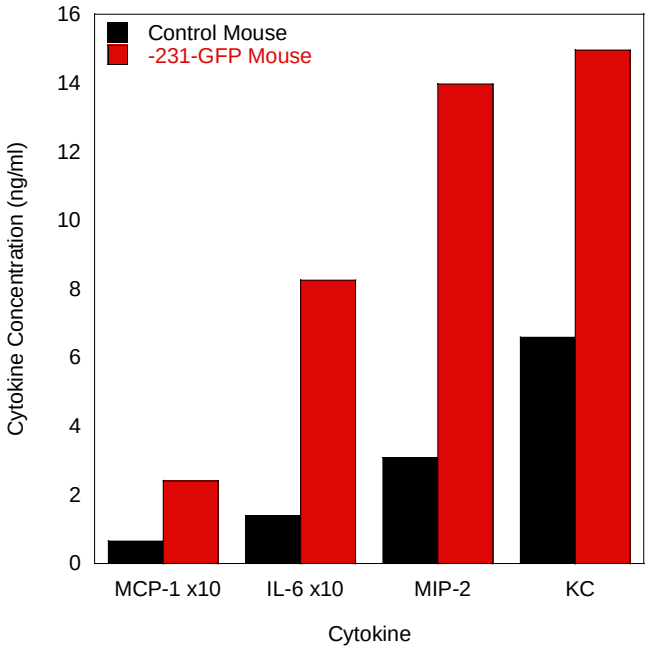

MDA-MB-231-GFP cells (3 x 10^5 cells) were inoculated into the left cardiac ventricle of 4-6 week old athymic, female mice. Control mice were untreated. Mice were euthanized at 4 weeks and femurs harvested. Femur metaphyses were fractionated. Isolated metasphyseal bone pieces were crushed and cultured. Media were collected and tested after 24 hours. Murine MCP-1 cytokine production was quantified using ELISAs. Murine IL-6, MIP-2, and KC were quantified using a Bio-Rad Bio-Plex™ murine cytokine quantification assay. Shown is a representative experiment.

Figure 10.: Cytokine expression of murine femur metaphyses ex-vivo following intracardiac inoculation with various human metastatic breast cancer cells.

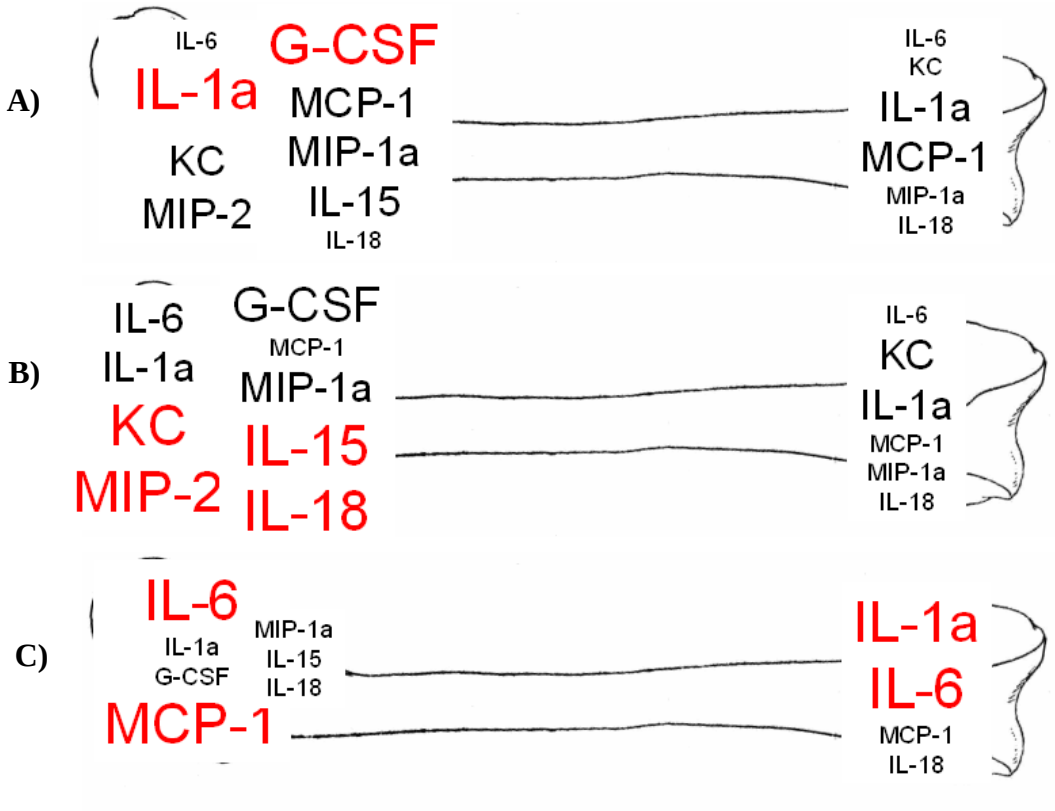

Control (A; nothing), MDA-MB-435-GFP (B), or MDA-MB-231-GFP cells (C) (3×10^5 cells) were inoculated into the left cardiac ventricle of 4-6 week old athymic, female mice. Control mice were untreated. Mice were euthanized at 4 weeks and femurs harvested. Femur metaphyses were fractionated. Isolated metasphyseal bone pieces were crushed and cultured. Media were collected and tested after 24 hours. Murine cytokine production was quantified a Bio-Rad Bio-Plex™ murine cytokine quantification assay. Cytokine concentration is represented by size; larger amounts are represented by larger font size. Cytokines listed in red were expressed in the greatest amounts.

Figure 11.: Cytokine expression of murine femur epiphyses ex-vivo following intracardiac inoculation with various human metastatic breast cancer cells.

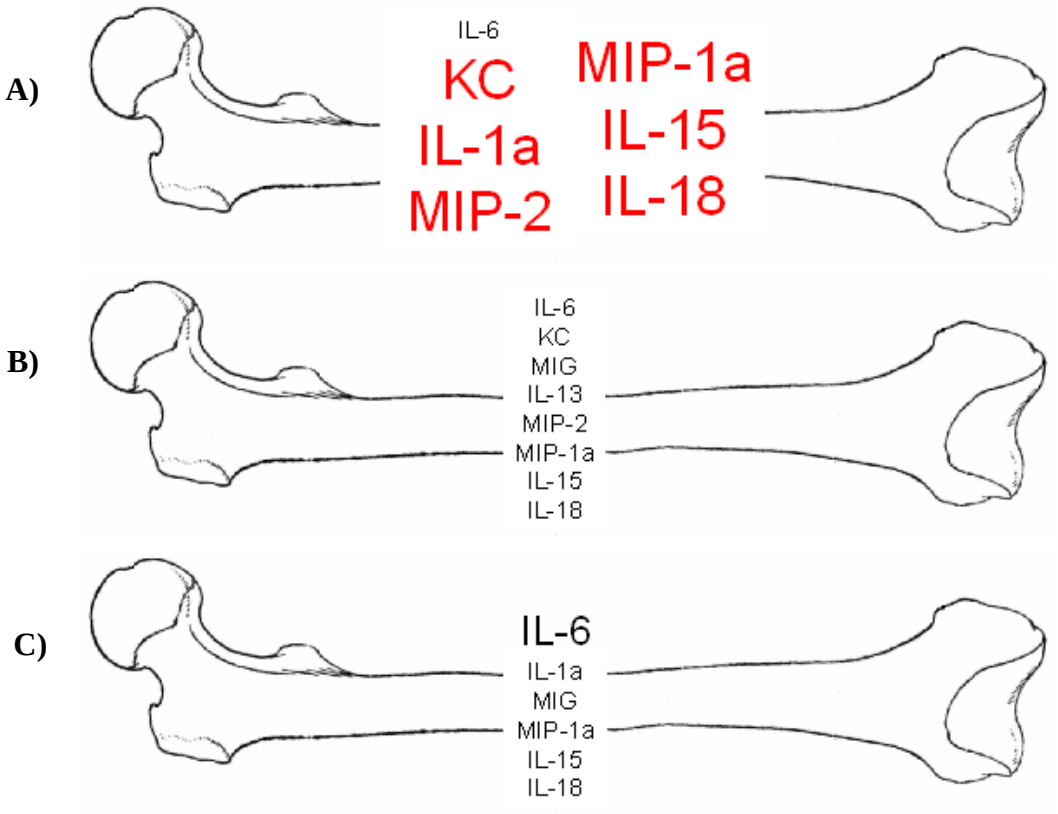

Control (A; nothing), MDA-MB-435-GFP (B), or MDA-MB-231-GFP cells (C) (3×10^5 cells) were inoculated into the left cardiac ventricle of 4-6 week old athymic, female mice. Control mice were untreated. Mice were euthanized at 4 weeks and femurs harvested. Femur metaphyses were fractionated. Isolated epiphyseal bone pieces were crushed and cultured. Media were collected and tested after 24 hours. Murine cytokine production was quantified a Bio-Rad Bio-Plex™ murine cytokine quantification assay. Cytokine concentration is represented by size; larger amounts are represented by larger font size. Cytokines listed in red were expressed in the greatest amounts.

Figure 12.: Summary of a possible interpretation of data collected in this report.

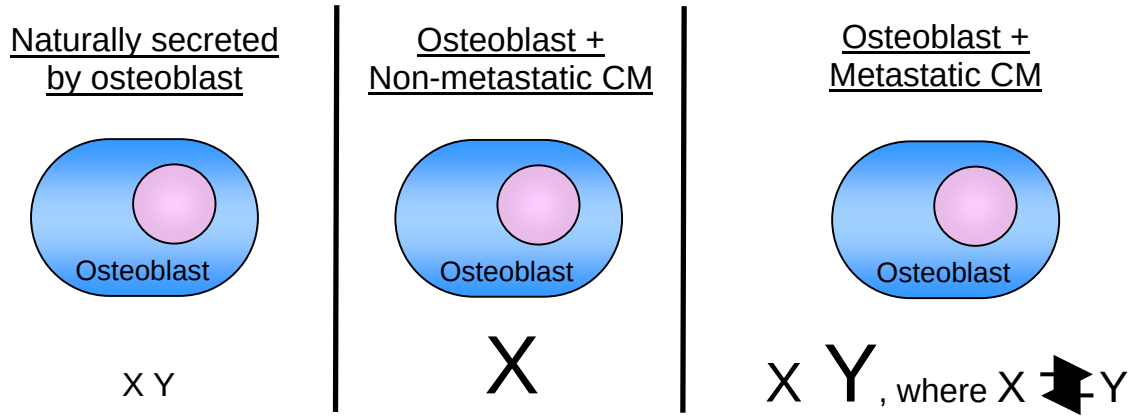

Crosstalk (⇄) between cells, bone-, and cancer-derived factors likely occurs and shifts the dynamics of the bone microenvironment to favor growth and development of metastatic breast cancer cells.

Table 1.: Alkaline phosphatase activity of MC3T3-E1 murine osteoblasts in transwell assay with MDA-231W or MDA-231GFP human metastatic breast cancer cells.

	Alkaline Phosphatase Activity at 4 Minutes (IU/L)			
Well	0.4 µm pore MDA-231GFP	0.4 µm pore MDA-231W	3 µm pore MDA-231GFP	3 µm pore MDA-231W
1	3.4	4.76	2.04	2.04
2	3.4	4.76	7.48	0.68
3	4.76	2.04	0	2.04

Alkaline phosphatase enzyme activity at 4 minutes of 11 day old MC3T3-E1 murine osteoblasts in a transwell system with MDA-231W or MDA-231GFP human metastatic breast cancer cells was assessed using an alkaline phosphatase enzyme kit (BioAssay Systems, Hayward, CA).

APPENDICES

1) Abstract: 2007 **Bussard, KM**, Mastro, AM. "Osteoblast-derived Inflammatory Cytokines are Produced in Response to Human Metastatic Breast Cancer Cells." The 100th Annual American Association for Cancer Research Annual Meeting, Los Angeles, CA, April 14-18, 2007. Proceedings of the 97th Annual Meeting for American Association for Cancer Research.

2) Publication: 2006 Phadke, PA, Mercer, RR, Harms JF, Jia, Y, Kappes, JC, Frost, AR, Jewell, JL, **Bussard, KM,** Nelson, S, Moore, C, Gay, CV, Mastro, AM, Welch, DR. "Kinetics of Metastatic Breast Cancer Cell Trafficking in Bone." Clinical Cancer Research. 12: (5) 1431.

3) Bussard, KM. Curriculum vitae.

Osteoblast-Derived Inflammatory Cytokines are Produced in Response to Human Metastatic Breast Cancer Cells

Breast cancer frequently metastasizes to bone. Although the precise mechanism underlying this preferential metastasis is unknown, bone likely provides a hospitable environment that attracts breast cancer cells and allows them to colonize and grow. Metastatic breast cancer cells induce osteoclast bone resorption, halt osteoblast bone deposition, and profoundly alter osteoblast properties. Current models suggest that chemokines and cytokines produced by breast cancer cells are key to understanding breast cancer metastasis. While cancer-derived cytokines may play an important role, we have evidence that *osteoblasts* can be directed by metastatic breast cancer cells to produce inflammatory cytokines that may be chemoattractants for both osteoclasts and cancer cells, as well as growth or maintenance factors for the cancer cells.

MC3T3-E1 murine osteoblasts (OB) were grown to different stages of differentiation (growth: 4 days, early differentiation: 10 days, and late differentiation: 20 days) and were treated for 24 hours with conditioned media (CM) from human metastatic breast cancer (BC) MDA-MB-231 cell variants (parental MDA-MB-231W, parental MDA-MB-231PY, bone-seeking MDA-MB-231BO, or brain-seeking MDA-MB-231BR). OB media was replaced with BC CM at 0, 10, 25, or 50%. Twenty-four hrs later, the culture media was collected and subjected to RayBio® mouse cytokine arrays and species-specific ELISAs to quantify OB-derived cytokines produced in response to human BC cells.

A RayBio® cytokine antibody array showed that BC CM treatment increased OB-derived inflammatory cytokine secretion. The increase in IL-6 levels was particularly notable. As quantitated by ELISAs, OB-derived IL-6 at day 4 doubled from control values when OBs were treated with MDA-MB-231BR CM. For days 10 and 20, OB-derived IL-6 was increased at least 10 fold over control values. Noteworthy increases in OB-derived IL-6 included greater than 80 fold increases from control values with the addition of 50% MDA-MB-231BR CM on day 10 and 50% MDA-MB-231PY CM on day 20. In summary, OB-derived IL-6 production increased in a dose-dependent manner with the addition of all types of BC CM at all points. Maximum induction of OB-derived IL-6 secretion occurred in more differentiated cells.

Literature suggests that IL-6 has numerous functions that could contribute to BC cell metastases to bone. These functions include effects on OBs, osteoclasts (OC), and BC cells. This study implicates OBs as an important source of IL-6 in the vicious cycle of BC bone metastasis. Comprehensive treatment of bone metastases must consider OBs, OCs, and BC cells in order to restore bone matrix deposition and limit osteolysis.

Supported by the U.S. Army Medical Research and Materiel Command (W81XWH-06-1-0363, W81XWH-06-1-0432), Susan G. Komen Breast Cancer Foundation (BCTR0601044), and National Foundation for Cancer Research, Center for Metastasis Research.

Authors: Karen M. Bussard and Andrea M. Mastro, The Pennsylvania State University, University Park, PA

Kinetics of Metastatic Breast Cancer Cell Trafficking in Bone

Pushkar A. Phadke,[1] Robyn R. Mercer,[6] John F. Harms,[1] Yujiang Jia,[2] Andra R. Frost,[1,3,5] Jennifer L. Jewell,[6] Karen M. Bussard,[6] Shakira Nelson,[6] Cynthia Moore,[1] John C. Kappes,[2] Carol V. Gay,[6] Andrea M. Mastro,[5,6] and Danny R. Welch[1,3,4,5]

Abstract

Purpose: *In vivo* studies have focused on the latter stages of the bone metastatic process (osteolysis), whereas little is known about earlier events, e.g., arrival, localization, and initial colonization. Defining these initial steps may potentially identify the critical points susceptible to therapeutic intervention.

Experimental Design: MDA-MB-435 human breast cancer cells engineered with green fluorescent protein were injected into the cardiac left ventricle of athymic mice. Femurs were analyzed by fluorescence microscopy, immunohistochemistry, real-time PCR, flow cytometry, and histomorphometry at times ranging from 1 hour to 6 weeks.

Results: Single cells were found in distal metaphyses at 1 hour postinjection and remained as single cells up to 72 hours. Diaphyseal arrest occurred rarely and few cells remained there after 24 hours. At 1 week, numerous foci (2-10 cells) were observed, mostly adjacent to osteoblast-like cells. By 2 weeks, fewer but larger foci ($\geq$50 cells) were seen. Most bones had a single large mass at 4 weeks (originating from a colony or coalescing foci) which extended into the diaphysis by 4 to 6 weeks. Little change ($<$20%) in osteoblast or osteoclast numbers was observed at 2 weeks, but at 4 to 6 weeks, osteoblasts were dramatically reduced (8% of control), whereas osteoclasts were reduced modestly (to $\sim$60% of control).

Conclusions: Early arrest in metaphysis and minimal retention in diaphysis highlight the importance of the local milieu in determining metastatic potential. These results extend the Seed and Soil hypothesis by demonstrating both intertissue and intratissue differences governing metastatic location. Ours is the first *in vivo* evidence that tumor cells influence not only osteoclasts, as widely believed, but also eliminate functional osteoblasts, thereby restructuring the bone microenvironment to favor osteolysis. The data may also explain why patients receiving bisphosphonates fail to heal bone despite inhibiting resorption, implying that concurrent strategies that restore osteoblast function are needed to effectively treat osteolytic bone metastases.

Authors' Affiliations: Departments of [1]Pathology and [2]Medicine-Hematology/Oncology, [3]Comprehensive Cancer Center, [4]Center for Metabolic Bone Disease, [5]National Foundation for Cancer Research, Center for Metastasis Research, University of Alabama at Birmingham, Birmingham, Alabama, and [6]Department of Biochemistry and Molecular Biology, Pennsylvania State University, University Park, Pennsylvania

Received 8/19/05; revised 11/1/05; accepted 12/15/05.

Grant support: U.S. Army Medical Research and Materiel Command (DAMD-17-02-1-0541, DAMD-17-03-01-0584, and DAMD 17-02-1-0358) and the University of Alabama at Birmingham Breast Specialized Programs of Research Excellence (P50-CA89019). Additional support was provided by CA87728, the National Foundation for Cancer Research, Center for Metastasis Research, and the Pennsylvania Department of Health Breast Cancer Program.

The costs of publication of this article were defrayed in part by the payment of page charges. This article must therefore be hereby marked *advertisement* in accordance with 18 U.S.C. Section 1734 solely to indicate this fact.

Note: P.A. Phadke and R.R. Mercer contributed equally to this work.

This work was submitted in partial fulfillment of the requirements for the University of Alabama at Birmingham Graduate Program in Molecular and Cellular Pathology (P.A. Phadke) and Penn State Graduate Program in Biochemistry and Molecular Biology (R.R. Mercer).

Requests for reprints: Danny R. Welch, Department of Pathology, University of Alabama at Birmingham, Volker Hall G-019A, 1670 University Boulevard, Birmingham, AL 35294-0019. Phone: 205-934-2961; Fax: 205-975-1126; E-mail: DanWelch@uab.edu.

doi:10.1158/1078-0432.CCR-05-1806

Breast cancer has a remarkable predilection to colonize bone, with an incidence between 70% and 85% in patients (1–3). At the time of death, metastatic bone disease accounts for the bulk of tumor burden (4). For women with bone metastases, the complications—severe, often intractable pain, pathologic fractures, and hypercalcemia—are catastrophic. Despite its obvious clinical importance, very little is understood about the fundamental mechanisms responsible for breast cancer metastasis to bone. Research progress has been hampered by the dearth of, and technical difficulties inherent in, the current models.

Most models of metastasis poorly recapitulate the pathogenesis of breast cancer. The ideal model would involve dissemination from an orthotopic site (i.e., mammary fat pad), colonization, and osteolysis. None of the currently available human breast xenograft models spread to bone following orthotopic implantation and only one murine model metastasizes to bone from the mammary fat pad (5). Furthermore, most human cell lines do not metastasize to bone in mice regardless of route of injection. The most commonly used model of breast cancer metastasis to bone involves injection of tumor cells into the arterial circulation via the left ventricle of the heart (4, 6–8). This route of injection minimizes first-pass filtration through pulmonary capillaries, thereby allowing more cells to reach the bone.

Current methods to detect bone metastases are insufficiently sensitive (e.g., radiography) or are impractical for adequately statistically powered experiments because of costs or labor-intensiveness. Radiography can detect osteolytic lesions only after more than half of the calcified bone matrix has been degraded (9). Microcomputerized tomography is not widely available, but is likewise of insufficient resolution to recognize single tumor cells. Serial sectioning (which would be required to locate rare single cells) is cost-prohibitive, except for small studies. As a result, experiments have been limited to late events of metastatic bone disease, such as osteolysis. Therefore, antecedent events (i.e., arrival, lodging, intraosseous trafficking, and colonization) have not been studied except by inference.

To overcome some of the technical limitations, more sensitive methods using reporter molecules, such as luciferase (10) or β-galactosidase (LacZ) have recently been described (11–13). Luciferase, although it allows for *in situ* detection of tumor cells in the bone, does not allow for microscopic localization of the cells. Because luminescence depends on a fully viable cell, use of luciferase is limited *ex vivo*. β-Galactosidase is excellent for studies at the histologic level but cannot be used for studies involving intact bone unless the lesions are macroscopic. Diffusion or distribution of substrate into bone is also a complication.

Fluorescent molecules, like enhanced green fluorescent protein (GFP), have also been employed with some success in the early detection of bone metastasis (14–16). We recently used the GFP-tagged MDA-MB-435 metastatic human breast cancer cell line to reveal formation of osteolytic bone lesions following intracardiac injection in athymic mice (15). Like luciferase, GFP can be used to detect lesions *in situ*, even though the limits of detection are restrictive (~0.5-1 mm). During experiments designed for other purposes, we detected single tumor cells in bone within minutes postinjection. Because to the best of our knowledge, no one had ever systematically studied the earliest tumor cell-bone interactions (except by serendipitous histologic sections), we decided to use the power of GFP to begin addressing the early events associated with breast tumor cells that have already disseminated to bone.

It has long been recognized that, once cells arrive in the bone, they alter homeostasis. Turnover of the skeleton is dynamic and continuous throughout embryonic development and adulthood. Calcified bone matrix turns over completely, on average, every decade (17, 18). Calcified matrix remodeling involves an interplay between osteoblasts (bone forming cells) and osteoclasts (bone resorbing cells). Altering the balance of activities results either in excessive bone deposition (osteopetrosis) or bone loss (osteoporosis). Although larger individual bone lesions contain regions that are both osteopetrotic and osteoporotic, most breast cancer bone metastases are not osteolytic. The current paradigm suggests that tumor cells influence osteoclast activity (4, 19). Using the GFP model of breast cancer metastasis to bone, we sought to identify key tumor cell–bone cell interactions (and the timing of those interactions) that occur during the pathogenesis of bone metastasis.

Materials and Methods

Cell lines and culture. Metastatic human breast carcinoma cell line, MDA-MB-435 (MDA-435), a generous gift from Dr. Janet Price (University of Texas M.D. Anderson Cancer Center, Houston, TX), was stably transfected with pEGFP-N1 (BD Biosciences Clontech, Palo Alto, CA) by electroporation (Bio-Rad Model GenePulser, Hercules, CA; 220 V, 960 μ Fd, $\infty\Omega$) or transduced with a HIV type 1-based, lentiviral vector system constitutively expressing enhanced GFP (20, 21). For the lentivirus, the GFP coding sequence was inserted into the vector 5′ of the internal ribosome entry site and puromycin sequences, each of which were under control of the early cytomegalovirus promoter. Infectious stock were prepared by transfection of 293T cells and used at a multiplicity of infection of ~10.

The origin of MDA-MB-435 has been questioned because the cells express melanoma-associated genes in cDNA microarray experiments. However, the patient was reported only to have a breast carcinoma. Because MDA-MB-435 cells express milk proteins (22), it is most simple to conclude that the cells are poorly differentiated breast carcinoma.

Parental cells were cultured in a mixture (1:1 vol/vol) of DMEM and Ham's F12 media (DMEM/F12; Invitrogen, Carlsbad, CA) supplemented with 2 mmol/L L-glutamine, 1 mmol/L sodium pyruvate, 0.02 mmol/L nonessential amino acids, 5% fetal bovine serum (Atlanta Biologicals, Norcross, GA), without antibiotics or antimycotics (cDME/F12). All cultures were confirmed to be negative for *Mycoplasma* spp. infection using a PCR-based test (TaKaRa, Shiga, Japan).

GFP-expressing cells were grown in cDME/F12 plus G418 (Geneticin, 500 μg/mL, Invitrogen) or puromycin (500 μg/mL, Fisher Scientific, Hampton, NH). The brightest 15% (lentiviral) or 25% (pEGFP) fluorescing cells were sorted using either Coulter EPICS V cell sorter (Beckman-Coulter, Fullerton, CA) or a BD FACSaria cell sorter (BD Biosciences Immunocytometry Systems, San Jose, CA).

Intracardiac injections. Cells at 80% to 90% confluency were detached using a mixture of 0.5 mmol/L EDTA and 0.05% trypsin in Ca^{+2}-, Mg^{+2}-, and $NaHCO_3$-free HBSS. Viable cells were counted using a hemacytometer and resuspended at a final concentration of 1.5×10^6 cells/mL in ice-cold HBSS. Cells were not used unless viability was >95%, but was usually >98%. Female athymic mice ages between 4 and 6 weeks (Harlan Sprague-Dawley, Indianapolis, IN) were anesthetized by i.m. administration of a mixture of ketamine-HCl (129 mg/kg), and xylazine (4 mg/kg). Cells (3×10^5 in 0.2 mL) were injected into the left ventricle of the heart between the third and fourth or between the fourth and fifth intracostal space. The presence of bright red, as opposed to burgundy, colored blood prior to and at the end of each inoculation confirmed injection of the entire volume into the arterial system. Mice were necropsied at 1, 2, 4, 8, 24, 48, and 72 hours and 1, 2, 4, and 6 weeks postinoculation following anesthesia with ketamine/xylazine and euthanasia by cervical dislocation. At least two independent experiments were done with 5 to 12 mice per experimental group. Not all time points were collected for every experiment.

Although widespread skeletal metastases develop after intracardiac injection (15, 23), the experiments reported here focused exclusively on the femur, a common site for metastasis that is easily accessible. The femurs were removed and examined by low magnification (×2-10) fluorescence stereomicroscopy and histologic and histomorphometric analyses (24, 25). Some femurs were divided into proximal and distal metaphyses plus cortical shaft (diaphysis) from which the marrow was collected and cells examined by flow cytometry or quantitative real-time PCR. Corroborating experiments were done with the contralateral femur to assure that there was no bias for sidedness.

Mice were maintained under the guidelines of the NIH, the University of Alabama at Birmingham, and the Pennsylvania State University. All protocols were approved and monitored by the appropriate Institutional Animal Care and Use Committees.

Fluorescence microscopy. To visualize metastases derived from the GFP-tagged cell lines, whole femurs (dissected free of soft tissue using a no. 11 scalpel blade with gauze used to grip and remove tissue remnants) were placed into Petri dishes containing ice-cold Ca^{+2}- and Mg^{+2}-free Dulbecco's PBS and examined by fluorescence microscopy using a Leica MZFLIII dissecting microscope with ×0.5 objective and

GFP fluorescence filters ($\lambda_{excitation}$ = 480 ± 20 nm; $\lambda_{emission}$, 510 nm barrier; Leica, Deerfield, IL). Photomicrographs were collected using a MagnaFire digital camera (Optronics, Goleta, CA), and ImagePro Plus 5.1 software (Media Cybernetics, Silver Spring, MD).

Bone fixation and storage. Intact, dissected femurs from individual mice were placed in 25 mL glass scintillation vials and fixed in freshly prepared 4% paraformaldehyde in Ca^{+2}- and Mg^{+2}-free Dulbecco's PBS or in periodate-lysine-paraformaldehyde solution (26) at 4°C for 24 to 48 hours. GFP fluorescence was difficult to maintain in fixed tissues and bone sections; however, we were able to overcome this limitation by maintaining the samples at 4°C (27). Bones destined for histologic sectioning were subsequently removed and decalcified in 0.5 mol/L EDTA in Ca^{+2}- and Mg^{+2}-free Dulbecco's PBS.

Bone histomorphometry. Bones were dehydrated in increasing concentrations of ethanol and embedded in a mixture of 80:20 methyl methacrylate and dibutylphthalate. Serial coronal sections (5 μm) were obtained using a Leica 2265 microtome. The distal ends of femurs (spongiosa) were analyzed. Sections were first stained with Sanderson's rapid bone stain for 2 minutes. Once tumor cells were identified, subsequent sections were stained with Goldner's trichrome and tartrate-resistant acid phosphatase (TRAP). Histomorphometry was done at the University of Alabama at Birmingham Center for Metabolic Bone Disease Histomorphometry and Molecular Analysis Core Facility by the method of Parfitt et al. (24, 25) using Bioquant image analysis software (R&M Biometrics, Nashville, TN).

Immunohistochemistry. Paraffin-embedded samples were sectioned (5 μm, coronal or sagittal), deparaffinized, and rehydrated before antigen retrieval by microwaving for ~8 minutes at full power (700 W) in a 10 mmol/L citrate buffer (pH 6). Samples were boiled for 5 minutes in the microwave oven. Endogenous peroxidase activity was blocked by treatment with 3% hydrogen peroxide for 5 minutes. Sections were blocked with 1% goat serum for 1 hour. Slides were incubated with primary rabbit polyclonal anti-GFP IgG (1:250; Molecular Probes, Eugene, OR) for 1 hour, followed by secondary biotinylated anti-rabbit antibody (TITRE; Level 2 Ultra Streptavidin Detection System, Signet Labs, Dedham, MA). Detection was achieved using Biogenex liquid DAB kit (Biogenex, San Ramon, CA) and slides were counterstained using hematoxylin. GFP-positive tumor samples served as positive controls. Negative controls were done by omitting the primary antibody.

Some femurs were fixed in a solution of 2% paraformaldehyde containing 0.075 mol/L lysine and 0.01 mol/L sodium periodate (pH 7.4), 4°C for 24 hours in an attempt to maintain alkaline phosphatase activity (26). Although the alkaline phosphatase activity was not well preserved, fluorescence was maintained; fluorescent MDA-435^{GFP} cells could be observed in femurs taken throughout the time course. Following decalcification as described above, the bones were embedded in paraffin. Paraffin-embedded bones were sectioned lengthwise into 10 μm sections and several sections throughout the bone were analyzed. The sections were deparaffinized, rehydrated, and stained for apoptotic cells with a modified terminal nucleotidyl transferase–mediated nick end labeling (TUNEL) procedure using Cy-5 rather than FITC-labeled dUTP (28). Bone sections were first scanned at ×20 magnification using a fluorescence confocal microscope. Areas in which GFP-positive cells were detected were further analyzed at ×40 magnification with both fluorescence and phase microscopy. Fluorescent images were captured at two wavelengths $\lambda_{excitation}$ = 480 ± 20 nm ($\lambda_{emission}$, 520 nm for GFP) and $\lambda_{excitation}$ = 647 nm ($\lambda_{emission}$, 670 nm for Cy-5). A comparison of the numbers of breast cancer cells detected by fluorescence microscopy versus use of anti-GFP gave essentially the same trends (data not shown).

TRAP-positive cells were determined in the femurs of mice at various times following inoculation with metastatic breast cancer cells. Two to eight sections from two to four bones per time period were stained for the presence of TRAP by immunohistochemistry (Sigma-Aldrich, St. Louis, MO). After staining, the sections were viewed with a fluorescent light microscope at ×20 magnification. Three images (1,349 pixels/500 μm) from the distal end and three images from the proximal end were collected and converted into JPEG format. The number of TRAP-positive cells was counted in each image. The Image J program (NIH) was used to calculate the bone area in each field.

Some decalcified femurs were cryosectioned and stained for alkaline phosphatase activity (Sigma-Aldrich). The sections were examined with a light microscope, the images digitally collected, and analyzed for the amount of alkaline phosphatase stain per area of bone at the growth plate and in the trabecular region. The data were calculated as ratio of the mm^2 of the alkaline phosphatase stain to mm^2 of bone.

Flow cytometric and DNA analysis. Femurs were removed from five to six mice at each time and cut into the distal and proximal metaphyses and the diaphysis. Bone marrow was flushed from these regions with a 1 mL tuberculin syringe fitted with a 26-gauge needle. The marrow in the center of the diaphysis was collected separately from the endosteal marrow close to the cortical bone as previously described (29). For flow cytometry, the RBC were lysed with ACK solution (15 mmol/L NH_4Cl, 1 mmol/L $KHCO_3$, 0.1 mmol/L Na_2 EDTA) and the remaining cells were fixed with 2% paraformaldehyde. Samples were stored at 4°C until they were analyzed by flow cytometry (Coulter XL-MCL) using standardized fluorescent beads (10 μm; Sphero AccuCount Rainbow Fluorescent particles, Spherotech, Libertyville, IL) to estimate the total number of cancer cells present. Standard curves were also generated by adding known numbers of MDA-MB-435 cells to mouse bone marrow cells. The samples of the mixtures of cells were prepared in the same way as the experimental samples. A background value of 200 cells was determined from the data obtained from the control animals in which no GFP-positive cells were present.

For DNA analysis, marrow was centrifuged and frozen in Ca^{+2}- and Mg^{+2}-free Dulbecco's PBS. At a later time, DNA was prepared from the samples with a DNeasy kit (Qiagen, Valencia, CA). The DNA was subjected to quantitative real-time PCR (Nucleic Acid Facility, Penn State, University Park, PA) using primers to detect the *HERVK* gene (human endogenous retrovirus, group K), a gene found in the human but not in the mouse genome (30). To establish a standard curve, MDA-435^{GFP} cells were counted, diluted, and added to preparations of mouse bone marrow cells. DNA was isolated from these samples and treated as the experimental samples for PCR. Although one cell could be detected in the standard curve samples, a more conservative cutoff of 150 cells was used due to practical considerations, i.e., cell extract volumes and variations in the amount of mouse DNA present in each sample.

Statistics. Each series of injections involved between 5 and 15 mice per experimental group or time. Femurs were apportioned for various subsequent analyses. Comparisons between groups were done by one-way ANOVA with Student-Neumann-Kuels or Tukey's post-tests. Statistical significance was defined as a probability $P \leq 0.05$.

Results

Kinetics of MDA-435^{GFP} tumor cells trafficking in the bone. Numerous solitary fluorescent cells could be visualized in the intact bone (i.e., the bone is not cut, but has been stripped of surrounding muscle) 1 hour following intracardiac injection using fluorescence microscopy (Fig. 1A1). The majority (>90%) of cells were found in the metaphyseal regions, not in the diaphysis, by fluorescence. Routine identification of single tumor cells using H&E stain, although possible, proved difficult. Even with evidence that tumor cells were present in the bone (i.e., by fluorescence), we could not always unambiguously identify single tumor cells in histologic sections stained by H&E.

To facilitate detection of solitary tumor cells by histology and to determine their positions within the trabeculae, cellular

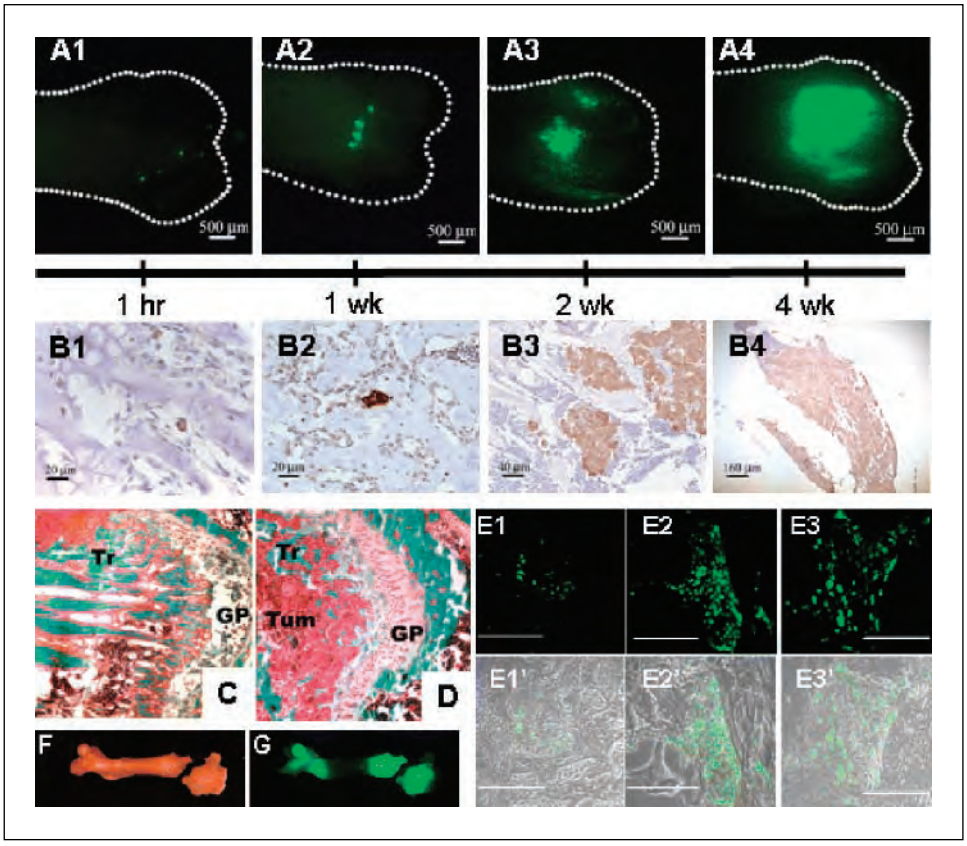

Fig. 1. The kinetics of MDA-435^{GFP} metastatic growth in the femur following intracardiac injection. Whole femurs were dissected and fluorescent foci were visualized in the intact bones using a fluorescent stereomicroscope. *A,* fluorescent foci were observed, mainly in the distal end of femurs, as shown at 1 hour (*A1*), 1 week (*A2*), 2 weeks (*A3*), and 4 weeks (*A4*). *B,* MDA-435^{GFP} cells were detected by anti-GFP immunohistochemistry (*brown staining cells*) in femurs at 1 hour (*B1*, single cell), 1 week (*B2*, clusters of two to three cells), 2 weeks (*B3*), and 4 weeks (*B4*). With time, the number of fluorescent foci decreased as the size increased. Independent tumor deposits often coalesced. *C* and *D,* representative images of distal ends of femur stained with Goldner's trichrome stain (*C,* normal bone; *D,* 4 weeks). The amount of trabecular bone (*Tr*, stained teal) is significantly lower in bone containing tumor cells, reflective of osteolytic degradation. Tumor cells (*Tum*) infiltrating the metaphyseal area near epiphyseal growth plate (*GP*) are labeled for reference. *E,* fluorescent tumor cell foci in trabecular bone in paraffin-embedded sections at 2 weeks (*E1*), 4 weeks (*E2*), and 6 weeks (*E3*) postinjection. Magnification line indicates 100 μm. E1′, E2′, and E3′ are composites of fluorescent and phase images. Representative bright field (*F*) and fluorescent (*G*) images of a mouse femur at 4 weeks show two large metastatic foci, one at each end. The distal end shows an iatrogenic fracture, presumably due to weakness caused by tumor cell – induced osteolysis.

location was estimated in two dimensions using fluorescence. Then, serial histologic sections were cut from the regions exhibiting fluorescence. Although this manipulation increased the odds of finding sections containing single cells, it was not always possible to detect cells in every 5 to 10 μm section stained using anti-GFP antisera. Nonetheless, as implied by the fluorescence data, most tumor cells were located in the primary spongiosa of the metaphysis of the distal femur (Fig. 1B and E). Although fluorescent cells were not frequently detected in the femoral head at 1 hour postinjection, some GFP-positive cells were detected by immunohistochemistry (data not shown). There was no evidence of unusual inflammation or immune cell infiltration at the sites of tumor cell arrest or colonization.

In a third, parallel approach, we detected cells without visualization constraints or sampling errors associated with sectioning, instead quantifying tumor cells in various marrow compartments using flow cytometry or real-time PCR. Separation of the marrow from metaphyses and diaphysis followed by flow cytometry or real-time PCR to detect MDA-435^{GFP} cells revealed a slightly different pattern of tumor cell distribution within the bone at the early times, but an entirely consistent pattern of distribution at the later times (Fig. 2). These methods were limited because precise separation of the diaphysis from the metaphysis was not consistent. Therefore, cancer cells at the interface between bone regions could not be localized with certainty. Histologic sections confirmed precise localization (Fig. 1). As a whole, the various methods to assess localization were largely confirmatory. In addition, we also determined that cancer cells in the diaphysis were mostly located next to the endosteal bone rather than in the marrow in the center of the shaft. By 4 to 6 weeks, >95% of tumor cells were found in the endosteal marrow (Fig. 5).

Of the 3×10^5 cells injected per mouse, a small fraction were detectable in the femurs (Table 1), as expected, because cells are distributed throughout the body following injection into the arterial circulation. Flow cytometry and real-time PCR were used to quantify the number of cells present. Cells were flushed from the marrow space in the metaphyseal and diaphyseal regions and examined by flow cytometry to detect GFP-tagged cells (Fig. 2). In addition, DNA isolated from the bone marrow was analyzed for the presence of human DNA by real-time PCR using a human-specific primer/probe set (Fig. 2). Regardless of the method, seeding of the femurs with breast cancer cells was rare (44 ± 6 cells; 0.01% per femur; Table 1). As a result, the absolute numbers were highly variable between mice and between techniques. Thus, the total number of single cells identified was not sufficient to perform statistical analyses with adequate power. Nonetheless, we did observe several consistent changes. First, solitary cells in the diaphysis were seldom detected beyond 24 hours in any of the mice, until metaphyseal lesions had apparently extended into the diaphyses at later times (Figs. 1G and 2). Second, the number of fluorescent foci (i.e., cell masses) detected by fluorescent stereomicroscopy decreased progressively beginning from 1 to 72 hours. This result is consistent with the clearance of disseminated tumor cells from other organs (31, 32). Third, single cells persisted in the femur for up to 72 hours. In general, evidence of cell division prior to 72 hours postinoculation was infrequent.

Whereas initial proliferation of arrested cells was delayed, distinct metastatic foci (5 ± 1) were easily detected by fluorescence microscopy of the intact bone (Fig. 1A2) as well as immunohistochemistry in the femur at 1 week (Fig. 1B2) and fluorescence microscopy of bone sections (Fig. 1E). Most of the foci were small and consisted of <10 cells (i.e., only three to four cell divisions). Although most metastatic lesions were localized at the distal end, a fraction of the bones had fluorescent foci growing at the proximal ends as well.

By 2 weeks, larger but fewer foci (2.8 ± 0.5) were detected at the distal end (Fig. 1A3 and B3). The foci were comprised of clusters of ~50 cells. These progressively increased in size and decreased in number to an average of one metastatic focus at 4 weeks, presumably by coalescence (Fig. 1A4, B4, and G). By 6 weeks, tumor cells directly extended into the diaphysis, and in some cases, the whole medullary canal was occupied by tumor. Histomorphometry of the lesions revealed loss of most trabecular bone by 4 to 6 weeks (compare Fig. 1D and Fig. 1C).

Tumor cell modification of the bone microenvironment. Histomorphometric analysis further showed specific modification of the microenvironment when tumor cells were present (Fig. 3). We had previously shown that MDA-435^{GFP} cells form radiographically detectable osteolytic lesions within 4 to 6 weeks following intracardiac injection (15). That finding was corroborated by histomorphometry showing that calcified bone volume decreased as tumor volume increased

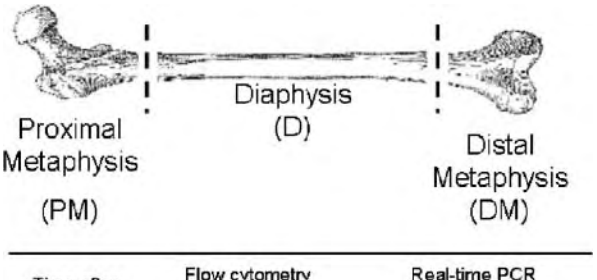

Time after injection	Flow cytometry			Real-time PCR		
	PM	D	DM	PM	D	DM
1 hr	1/5	2/5	0/5	4/5	3/5	2/5
4hr	2/5	2/5	0/5	4/5	4/5	3/5
24 hr	0/5	0/5	0/5	0/4	4/4	0/4
72 hr	2/5	1/5	2/5	2/5	4/5	1/5
1 wk	1/5	1/5	0/5	3/5	5/5	4/5
4 wk	2/5	2/5	3/5	4/5	5/5	5/5
6wk	0/3	1/3	2/3	2/3	3/3	3/3

Femoral ends were separated from the shaft with scissors. The proximal (PM) and distal (DM) metaphyses and the diaphysis (D) were flushed with ice-cold saline. Cells were collected and prepared for flow cytometry or DNA isolation and subsequent analysis by real-time PCR using HERVK, a human-specific gene. In practice, the limit of detection of MDA-435^{GFP} cells by flow cytometry was ~200 cells; by PCR it was ~150 cells. Shown are the numbers of animals in which the cancer cells were detected at various times and the bone areas in which they were found. The denominator is the number of bones examined at each time. Please note: the data presented are incidence only. The calculated number of cells is presented in Table 1 for each time.

Fig. 2. Detection of MDA-435^{GFP} metastatic cells by flow cytometry or real-time quantitative PCR in the metaphyseal and diaphyseal ends of the femur at various times following intracardiac inoculation.

Table 1. Retention of MDA-435^{GFP} cells in the femur following intracardiac injection

Time postinjection	Number of MDA-435^{GFP} cells in the femur
	Geometric mean (±1 SD)
1 h	41 (16-104)
4 h	54 (5-529)
24 h	40 (7-270)
72 h	44 (11-180)
1 wk	41 (20-82)
4 wk	11,271 (2,893-43,915)

NOTE: Marrow containing tumor cells was isolated from femurs as described in Materials and Methods. The number of MDA-435^{GFP} cells was determined by real-time quantitative PCR using probes for the human gene, HERVK. Shown are log-transformed data for four to five mice per group and only mice containing MDA-MB-435^{GFP} cells were included in the analysis.

(Fig. 3A). A decrease of 97% in the ratio of osteoid surface to bone surface at the 4-week point to osteoblast loss or loss-of-function as a major contributor to the decrease in calcified bone volume. This finding is consistent with previous work showing that MDA-MB-435 and MDA-MB-231 cells induce osteoblast apoptosis (33) and retard osteoblast differentiation (34) *in vitro*.

Importantly, osteoblast number per trabecular bone surface area in the metastatic lesions decreased with time (Fig. 3B). Bones from uninjected, age-matched mice served as negative controls. By 2 weeks, the number of osteoblasts decreased by ~20% in tumor-bearing mice. By 4 weeks, however, the decrease was more dramatic (~92% decrease; Fig. 3B). The decrease in osteoblast number was accompanied by an increase in the number of apoptotic osteoblasts observed by TUNEL (Figs. 3D and G, and 4A). Apoptotic osteoblasts were found at both proximal and distal ends of the femur, but little change in the number of apoptotic osteoblasts was observed in the diaphysis until tumor cells were routinely observed in that portion of the bone (Fig. 4A). This finding suggested that osteoblast apoptosis was occurring mostly when tumor cells were present. Supporting this hypothesis, TUNEL-positive osteoblasts were found almost exclusively in the presence (≤50 μm) of GFP-positive breast cancer cells (Figs. 3G and 4B). Previous (33) and current experiments (data not shown) have shown almost no tumor cell apoptosis when adjacent to osteoblasts. Bone sections stained for alkaline phosphatase, a marker for osteoblasts, showed a dramatic decrease as tumor burden increased (Fig. 3H-J). The ratio of the area occupied by alkaline phosphatase-positive cells per area of trabecular bone in the femurs of cancer-bearing mice was significantly lower compared with healthy mice (2.0 ± 0.6 versus 9.6 ± 1.7, respectively; $P \leq 0.0001$). In contrast, alkaline phosphatase activity in chondrocytes located in the growth plate was not significantly different (control, 25.9 ± 4.7; tumor bearing, 24.1 ± 5.0).

The number of osteoclasts remained unchanged at 2 weeks, but unexpectedly, a consistent decrease (~35-40% or to 60%

of control) in osteoclast number was observed at later times (Fig. 3C). This difference was evident by both quantitative histomorphometric analysis (Fig. 3C) and TRAP staining (Fig. 3E and F). The absolute number of both cell populations decreased so that the ratio of osteoblasts to osteoclasts decreased from an average of 40 to only 4 by 4 weeks.

Discussion

Bone is the most common site for metastases from breast carcinomas and their sequela account for approximately two-thirds of the costs associated with treating women with the disease (4, 36). As with most metastases, symptoms occur relatively late in disease progression. Whereas prevention of metastases altogether is ideal, restriction of progression to an asymptomatic state would improve clinical management of breast cancer. Likewise, repair of already existing lesions would benefit patients whose disease progression has been halted. As a result, understanding the antecedent steps for bone metastasis and osteolysis should provide insights for developing therapeutic interventions.

The results presented here are, to the best of our knowledge, the first to describe the behavior of breast cancer cells at the earliest times after they have arrived in the femur. Although the femur may not represent the behavior of tumor cells in all bones, it is a common site of secondary colonization both in patients with breast cancer and in experimental models. Therefore, we considered it an appropriate site for studying the process.

Single tumor cells were detected in the femur 1 hour after introduction into the arterial circulation (Fig. 5B). It is noteworthy that, even at this early time, tumor cells arrested primarily in the metaphyses rather than diaphyses. Although it is possible that differential expression of adhesion molecules may be found in metaphyseal versus diaphyseal bone

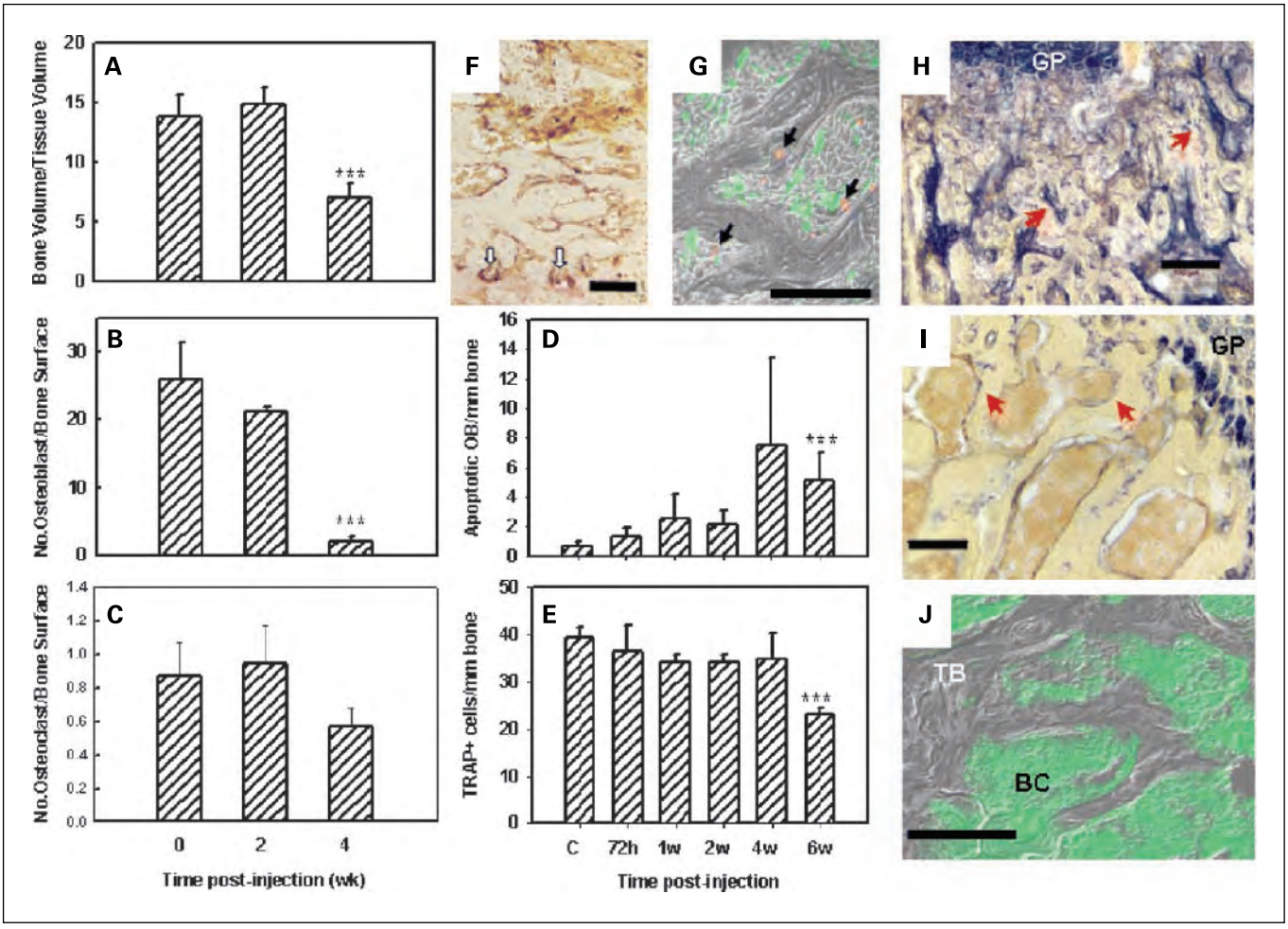

Fig. 3. MDA-435^{GFP} breast cancer cells diminished osteoblast and osteoclast numbers in colonized bone as evaluated by quantitative bone histomorphometry, immunohistochemistry, and fluorescent microscopy. *A-C,* histomorphometric analyses (*A,* bone volume to tissue volume; *B,* number of osteoblast per bone surface; *C,* number of osteoclast per bone surface). *D,* the number of apoptotic osteoblast (TUNEL-positive) per linear bone surface at times following inoculation of tumor cells. *E,* the number of osteoclasts (staining for TRAP) per linear bone surface at times following inoculation of tumor cells. *A-E,* significantly different ($P \leq 0.05$) from normal bone. *F,* representative image of osteoclast staining for TRAP (*red stain with white arrows*) taken from a section of femur 2 weeks after tumor cell inoculation. *G,* merged photomicrograph of MDA-435^{GFP} tumor cells (*green*) surrounding apoptotic osteoblast (*red*, TUNEL using Cy-5 probe) taken from a femur 6 weeks following inoculation. *H, I, J,* cryosections from a femur taken 4 weeks after tumor inoculation. *H,I,* stained for alkaline phosphatase activity (*blue staining by red arrows*) indicative of osteoblast; *J,* merged fluorescent and phase images showing trabecular bone (*TB*) surrounded by MDA-435^{GFP} cells (*BC*). Alkaline phosphatase activity was greatly diminished in the trabecular bone of tumor-bearing femurs but was still present in the growth plate (*GP*). Bars, 100 μm.

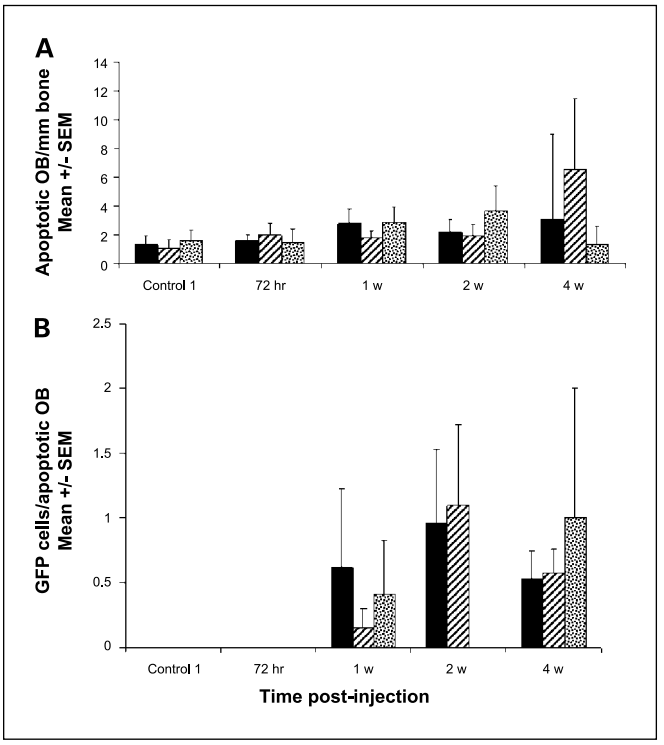

Fig. 4. The presence of metastatic breast cancer cells in close proximity to apoptotic osteoblasts increased with time following inoculation of MDA-435^{GFP}. *A,* apoptotic osteoblasts, detected by TUNEL, were counted in proximal and distal ends of paraffin sections of femur at times following tumor cell inoculation. *B,* number of MDA-435^{GFP} cells within a 50 μm radius of each apoptotic osteoblast. Averages from three femurs per time period. Proximal femur (*hatched columns*), distal femur (*stippled columns*), average over femur (*solid columns*). Apoptotic osteoblasts in the diaphyses were extremely rare.

vasculature (reviewed in ref. 37), anatomic and physiologic mechanisms are also likely to be important factors. Approximately 90% of the blood flow goes to the metaphyseal regions whereas a smaller fraction is found in the diaphyses (reviewed in ref. 38). Additionally, blood flow in the diaphysis is still largely vessel-based, whereas in the metaphyses, it is more sinusoidal. In the sinusoids, the rate of blood flow is <10% of that found in capillaries or other vessels (reviewed in ref. 37). Because of the sluggish blood flow, weaker adhesion molecules would not be subject to negative selection as when cells experience stronger sheer forces. However, arrest is not the only variable involved. The relatively rare cells initially seeding the diaphysis fail to remain there for prolonged periods. It is also possible that cancer cells follow a gradient of growth factors or cytokines. We have preliminary evidence[7] that several cytokines are found at much greater concentrations in the metaphysis compared with the diaphysis. The limitations of the present study cannot discriminate between loss of tumor cells to immune killing, apoptosis, sheer forces, etc., versus migration of tumor cells from the diaphysis to the metaphysis.

The earliest arriving tumor cells were mostly located in close proximity to osteoblasts and the bone-lining cells (Fig. 1B). In general, although the animal-to-animal variability was considerable, the majority of cells tended to be in the endosteal marrow, rather than in central marrow (Fig. 5G), suggesting that traversal from the sinusoids to trabecular space occurs relatively rapidly. This pattern is similar to that reported for hematopoietic precursors in bone marrow (29). Regardless of intra-osseous location, the trend was for tumor

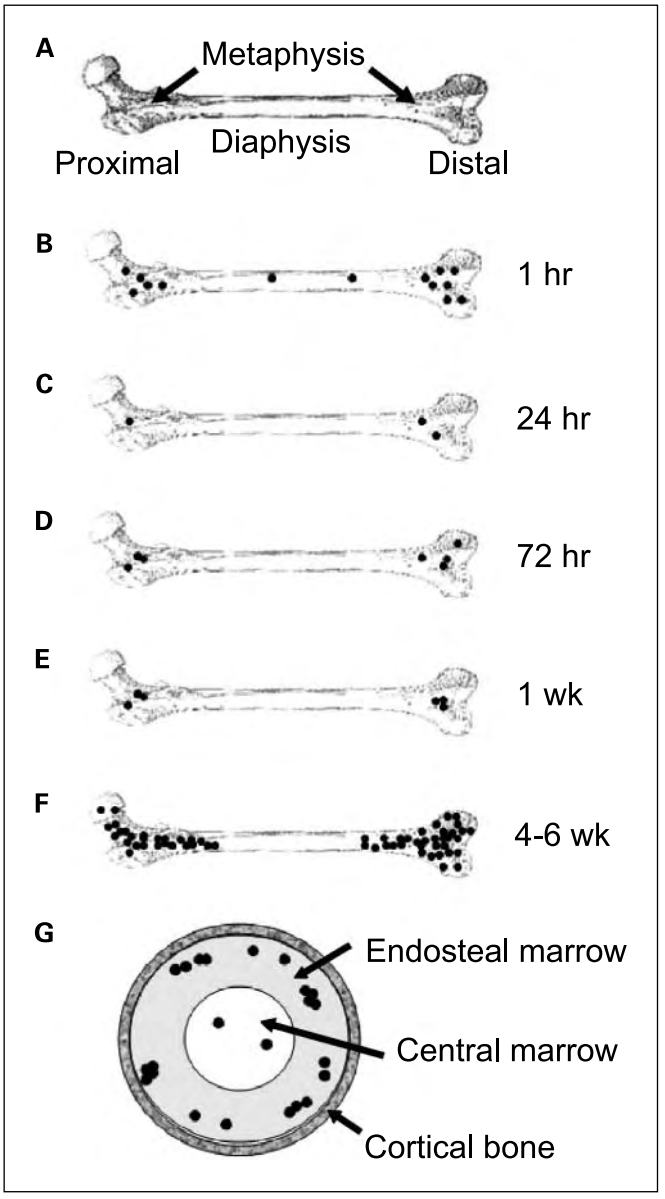

Fig. 5. Schematic diagram depicting colonization of the femur by MDA-435^{GFP} cells. A normal femur is diagramed and labeled for reference (*A*). Single cells (●) arrive in the bone marrow within 1 hour after intracardiac injection (*B*), with a distribution proportionate to the relative blood flow to regions of the bone. Most cells arresting in the bone are cleared within 24 hours (*C*). Of those remaining, the vast majority are still single cells but all are located in the metaphyses. A fraction of the surviving cells begin to proliferate by 72 hours (*D*) with little change in the number of foci, or size of tumor cell clusters, at 1 week postinoculation (*E*). The lesions progressively grow in size so that by 4 to 6 weeks, the mass of the metastases is large and the number of independently seeded cells are indiscernible because the foci have coalesced. Despite not seeding and remaining in the diaphyses, metastases extends into the bone shaft as the lesions grow (*F*). Flushing of bone marrow in established metastases as depicted in Fig. 2, revealed that most of the tumor cells are found in endosteal marrow (~90%) or in the central marrow (~10%), but never in the cortical bone of the diaphysis, as depicted in a cross-sectional view (*G*).

[7] A.M. Mastro, K.M. Bussard, and L. Shuman, unpublished observations.

cell numbers to decline during the first 72 hours after arrival (Fig. 5C and D).

It was somewhat surprising to find that most tumor cells had not begun to proliferate within 72 hours because proliferation typically begins much sooner (i.e., <48 hours) in lungs and orthotopic sites.[8] The period of quiescence or dormancy could be relevant because recent clinical studies have shown that 20% to 100% of women with breast cancer have evidence of disseminated tumor cells in the skeleton (35, 39, 40). Disseminated occult tumor cells within bone are thought to be in a sanctuary from which tertiary metastases could form and are thought to be responsible for late (sometimes months or years) recurrences. Based on abundant evidence from multiple experimental models, the fraction of disseminated cells progressing to overt metastasis is small. However, the presence of disseminated cells predicts poor prognosis in many tumor types, emphasizing that their presence at non-orthotopic sites should not be ignored (39, 40).

What triggers the conversion from dormant to proliferative cells remains unknown and is the subject of intense current investigation. The data presented here do not clarify the mechanistic issue, except to note that there is a substantial delay (72 hours) before the breast carcinoma cells begin to divide. Perhaps, during that time, tumor cells are altering the microenvironment. At our limits of detection, we could not tell whether there was balanced division (i.e., one of two of the progeny died or were eliminated) or whether tumor cells were adapting to the bone microenvironment prior to initiating growth. Upon arriving at a secondary site, tumor cells may remain dormant, undergo a limited number of cell divisions, or continue proliferating to form an overt mass. Presumably, the decisions are based on the response to signal(s) from the local microenvironment. There are self-evident cues that the tissue environment controls the development of bone metastasis based on the patterns of metastasis observed—e.g., metaphyseal > diaphyseal; distal > proximal; endosteal marrow > central marrow. The findings support and extend Stephen Paget's Seed and Soil hypothesis, by which he explains the predilection of breast carcinomas to colonize bone over other tissues (41). In short, Paget posited that tumor cells (seeds) were best suited for growth only in certain tissues (soils). The data presented here indicate that the soil may differ even within individual bones. Indeed the patterns of clinical bone metastases show marked preference for proximal and trabecular bone compared with distal or cortical bone (4). Surprisingly, the metastases arising from injection of MDA-435^{GFP} cells showed the opposite pattern—a slight, but consistent, penchant for distal, compared with proximal, femur. The pattern was consistent regardless of the method used to detect tumor cells. Hence, trivial experimental variables cannot explain why, in this model, metastases develops in the distal femur with greater frequency. One possibility invokes anatomic differences between mice and humans. Mice have extremely different gaits and mechanical pressures on their joints. Because tumor cells are generally predisposed to colonize injured tissues, biomechanical stresses on the knees in mice could, in part, explain the difference in arrest and colonization patterns between the species.

Notwithstanding preferential arrest/adhesion and growth in the metaphyses, metastatic breast carcinoma cells could still survive and grow in the diaphyses when the metastatic lesions are large enough. This growth pattern may suggest that tumor cells renovate the bone microenvironment sufficiently to reduce (or eliminate?) negative signals or that they can induce the production of positive factors from local, nontumor cells. Whether neoplastic cells have surpassed a threshold number, or whether some negative influence on tumor cells has been overcome, the incapacity to colonize diaphyses is not absolute.

It is widely accepted that metastatic breast carcinoma cells manipulate the bone microenvironment to induce osteolysis. In particular, tumor cell activation of osteoclasts via the "vicious cycle" of secretion of PTHrP or RANK ligand has been implicated in bone resorption (4, 19, 42). However, we previously hypothesized that the balance of bone deposition and resorption could be altered as well by reducing osteoblast number or differentiation and/or activity (33). *In vitro* coculture of metastatic human breast carcinoma cells or their conditioned medium with human osteoblasts resulted in apoptosis of the osteoblasts (33). The *in vivo* data presented here extend the previous findings by demonstrating that osteoblasts in the regions colonized by MDA-435^{GFP} are also eliminated.

It is possible that changes in the ratio of osteoblasts to osteoclasts in tumor-infiltrated bone tilts the balance in favor of increasing osteoclastic activity, thereby promoting osteolysis. The dramatic decrease in osteoblasts observed by 4 weeks prompted closer examination of osteoblast apoptosis at multiple times using TUNEL. The number of apoptotic osteoblasts progressively increased until later times, perhaps due to the already decreased number of osteoblasts. Interestingly, at earlier times (<4 weeks) at least one tumor cell was in direct contact (≤50 μm) with each TUNEL-positive osteoblast (Figs. 3E and 4B). Although this finding does not prove that tumor cells directly induce apoptosis, the data are consistent with this hypothesis. We also found with *in vitro* studies that breast cancer cell–conditioned medium prevented osteoblasts from differentiating as evidenced by lack of production of alkaline phosphatase, osteocalcin, and bone siaoloprotein (34). In this current study, the lack of alkaline phosphatase activity (Fig. 3H and I) may be due, in part, to failure of preosteoblasts to differentiate as well as apoptosis of mature osteoblasts. In either case, the outcome is the same, lack of functional osteoblasts.

Ours is the first *in vivo* evidence that tumor cells influence not only osteoclasts, as widely believed and showed, but also osteoblasts. The findings may explain, in part, the failure of bisphosphonate-treated patients to repair osteolytic bone lesions (43)—i.e., if there are no osteoblasts to reconstitute the bone, the lesions will remain.

It was surprising that osteoclast numbers were dramatically reduced in late-stage bone metastasis. Perhaps it should not have been because Orr, Mundy, and colleagues previously described that tumor cells themselves (i.e., in the absence of osteoclasts) could resorb bone (44, 45). The published data, although somewhat controversial, and the evidence presented here leave open the possibility that further progression of osteoclast-initiated osteolysis is possible. Furthermore, previous publications have shown significantly diminished osteoblast and osteoclast numbers in late stage breast carcinoma

[8] Unpublished observations.

metastasis to bone (46–48). Based on heterogeneity among tumors for multiple variables, molecular mechanisms of bone metastasis may vary while yielding the same end point, osteolysis.

A potential criticism of the reported work is that the findings are based on a single cell line. Given the heterogeneity of tumors and the redundant mechanisms from which each can choose to accomplish a given task, we are careful not to overgeneralize. Nonetheless, most key observations reported here have been replicated in the MDA-MB-231 breast carcinoma model of bone metastasis. MDA-MB-231 cells form osteolytic lesions with similar distribution as those found in MDA-MB-435. With expansion of bone lesions, osteoblast numbers decrease in MDA-MB-231 as well.[9] Assuming that the essential elements of osteolytic metastasis are observed in multiple breast carcinoma models, the findings reported here have significant implications with regard to control of bone metastasis in the clinic.

Foremost, the osteoblast is key. Whereas tumor cells could initiate growth prior to osteolysis, one of the earliest observed changes is the elimination of bone-forming cells. Even if bone resorption is controlled exogenously (i.e., by treatment with bisphosphamates), repair of defects is not possible. Because the structural integrity of the skeleton is critical to survival and quality of life, comprehensive treatment needs to restore bone matrix as well as limit osteolysis. By studying the trafficking of tumor cells within the bone and the effect of their presence on normal bone physiology, insights regarding how to improve control of bone metastasis will be forthcoming. Since the submission of this article, a report (49) describing a role for Dickkopf-1 in a Wnt-mediated pathway in prostate cancer cell osteoblastic lesions was published. Whether breast cancer–mediated osteolysis via impairment of osteoblast function is regulated by Dickkopf-1 or other components of the Wnt signaling pathway remains to be determined.

[9] P.A. Phadke and D.R. Welch, unpublished observations.

Acknowledgments

We are indebted to the superb technical assistance from Virginia R. Gilman as well as Patti Lott at the University of Alabama at Birmingham, Center for Metabolic Bone Disease Histomorphometry Core Facility, the University of Alabama at Birmingham Breast Specialized Programs of Research Excellence Tissue Core Facility, Deborah Grove and the Penn State Nucleic Acid Core Facility, and the Penn State Electron Microscopy and Histology Core Facility. We appreciate the critical reading of the manuscript and helpful suggestions from Dr. Tom Clemens.

References

1. Body JJ. Metastatic bone disease: clinical and therapeutic aspects. Bone 1992;13:S57–62.
2. Coleman RE. Skeletal complications of malignancy. Cancer 1997;80:1588–94.
3. Coleman RE, Rubens RD. The clinical course of bone metastases from breast cancer. Br J Cancer 1987;55:61–6.
4. Mundy GR. Metastasis: metastasis to bone: causes, consequences and therapeutic opportunities. Nat Rev Cancer 2002;2:584–93.
5. Lelekakis M, Moseley JM, Martin TJ, et al. A novel orthotopic model of breast cancer metastasis to bone. Clin Exp Metastasis 1999;17:163–70.
6. Chirgwin JM, Guise TA. Molecular mechanisms of tumor-bone interactions in osteolytic metastases. Crit Rev Eukaryot Gene Expr 2000;12:159–78.
7. Guise TA. Parathyroid hormone-related protein and bone metastases. Cancer 1997;80:1572–80.
8. Yoneda T, Sasaki A, Mundy GR. Osteolytic bone metastasis in breast cancer. Breast Cancer Res Treat 1994;32:73–84.
9. Averbuch SD. New bisphosphonates in the treatment of bone metastases. Cancer 1993;72:3443–52.
10. Wetterwald A, van der Pluijm G, Que I, et al. Optical imaging of cancer metastasis to bone marrow—a mouse model of minimal residual disease. Am J Pathol 2002;160:1143–53.
11. Holleran JL, Miller CJ, Culp LA. Tracking micrometastasis to multiple organs with *lacZ*-tagged CWR22R prostate carcinoma cells. J Histochem Cytochem 2000;48:643–51.
12. Amhlaoibh RN, Hoegh-Andersen P, Brünner N, et al. Measurement of tumor load and distribution in a model of cancer-induced osteolysis: a necessary precaution when testing novel anti-resorptive therapies. Clin Exp Metastasis 2004;21:65–74.
13. Sung V, Cattell DA, Bueno JM, et al. Human breast cancer cell metastasis to long bone and soft organs of nude mice: a quantitative assay. Clin Exp Metastasis 1997;15:173–83.
14. Murphy BO, Joshi S, Kessinger A, Reed E, Sharp JG. A murine model of bone marrow micrometastasis in breast cancer. Clin Exp Metastasis 2002;19:561–9.
15. Harms JF, Welch DR. MDA-MB-435 human breast carcinoma metastasis to bone. Clin Exp Metastasis 2003;20:327–34.
16. Yang M, Baranov E, Jiang P, et al. Whole-body optical imaging of green fluorescent protein-expressing tumors and metastases. Proc Natl Acad Sci U S A 2000;97:1206–11.
17. Manolagas SC. Birth and death of bone cells: basic regulatory mechanisms and implications for the pathogenesis and treatment of osteoporosis. Endocr Rev 2000;21:115–37.
18. Parfitt AM. Osteonal and hemi-osteonal remodeling: the spatial and temporal framework for signal traffic in adult human bone. J Cell Biochem 1994;55:273–86.
19. Roodman GD. Mechanisms of disease: mechanisms of bone metastasis. N Engl J Med 2004;350:1655–64.
20. Van Tine BA, Kappes JC, Banerjee NS, et al. Clonal selection for transcriptionally active viral oncogenes during progression to cancer. J Virol 2004;78:11172–86.
21. Chen W, Wu X, Levasseur DN, et al. Lentiviral vector transduction of hematopoietic stem cells that mediate long-term reconstitution of lethally irradiated mice. Stem Cells 2000;18:352–9.
22. Sellappan S, Grijalva R, Zhou XY, et al. Lineage infidelity of MDA-MB-435 cells: expression of melanocyte proteins in a breast cancer cell line. Cancer Res 2004;64:3479–85.
23. Harms JF, Welch DR, Samant RS, et al. A small molecule antagonist of the α-v, β-3 integrin suppresses MDA-MB-435 skeletal metastasis. Clin Exp Metastasis 2004;21:119–28.
24. Parfitt AM. Bone histomorphometry: proposed system for standardization of nomenclature, symbols, and units. Calcif Tissue Int 1988;42:284–6.
25. Parfitt AM, Drezner MK, Glorieux FH, et al. Bone histomorphometry: standardization of nomenclature, symbols, and units. Report of the ASBMR Histomorphometry Nomenclature Committee. J Bone Miner Res 1987;2:595–610.
26. Miao D, Scutt A. Histochemical localization of alkaline phosphatase activity in decalcified bone and cartilage. J Histochem Cytochem 2002;50:333–40.
27. Harms JF, Budgeon LR, Christensen ND, Welch DR. Maintaining green fluorescent protein tissue fluorescence through bone decalcification and long-term storage. Biotechniques 2002;33:1197–200.
28. Jewell J, Mastro AM. Using terminal deoxynucleotidy transferase (TDT) enzyme to detect TUNEL-positive, GFP-expressing apoptotic cells. Appl Cell Notes 2002;3:13–4.
29. Mason TM, Lord BI, Hendry JH. The development of spatial distributions of CFU-S and *in vitro* CFC in femora of mice of different ages. Br J Haematol 1989;73:455–61.
30. Mager DL, Medstrand P. Retroviral repeat sequences. In: Anonymous encyclopedia of the human genome. London: Macmillan Publishers Ltd., Nature Publishing Group; 2003. p. 1–7.
31. Goldberg SF, Harms JF, Quon K, Welch DR. Metastasis-suppressed C8161 melanoma cells arrest in lung but fail to proliferate. Clin Exp Metastasis 1999;17:601–7.
32. Fidler IJ. Metastasis: quantitative analysis of distribution and fate of tumor emboli labeled with ^{125}I-5-iodo-2′-deoxyuridine. J Natl Cancer Inst 1970;45:773–82.
33. Mastro AM, Gay CV, Welch DR, et al. Breast cancer cells induce osteoblast apoptosis: a possible contributor to bone degradation. J Cell Biochem 2004;91:265–76.
34. Mercer RR, Miyasaka C, Mastro AM. Metastatic breast cancer cells suppress osteoblast adhesion and differentiation. Clin Exp Metastasis 2004;21:427–35.
35. Masuda TA, Kataoka A, Ohno S, et al. Detection of occult cancer cells in peripheral blood and bone marrow by quantitative RT-PCR assay for cytokeratin-7 in breast cancer patients. Int J Oncol 2005;26:721–30.
36. Lipton A. Management of bone metastases in breast cancer. Curr Treat Options Oncol 2005;6:161–71.
37. Welch DR, Harms JF, Mastro AM, Gay CV. Breast cancer metastasis to bone: evolving models and research challenges. J Musculoskelet Neuronal Interact 2003;3:30–8.
38. Gross TS, Clemens TL. Vascular control of bone remodeling. In: Anonymous advances in organ biology. JAI Press Inc.; 1998. p. 138–60.
39. Pantel K, Woelfle U. Micrometastasis in breast cancer and other solid tumors. J Biol Regul Homeost Agent 2004;18:120–5.
40. Pantel K, Brakenhoff RH. Dissecting the metastatic cascade. Nat Rev Cancer 2004;4:448–56.
41. Paget S. The distribution of secondary growths in cancer of the breast. Lancet 1889;1:571–3.
42. Lynch CC, Hikosaka A, Acuff HB, et al. MMP-7

promotes prostate cancer-induced osteolysis via the solubilization of RANKL. Cancer Cell 2005;7: 485–96.

43. Lipton A, Theriault RL, Hortobagyi GN, et al. Pamidronate prevents skeletal complications and is effective palliative treatment in women with breast carcinoma and osteolytic bone metastases—long term follow-up of two randomized, placebo-controlled trials. Cancer 2000;88:1082–90.

44. Eilon G, Mundy GR. Direct resorption of bone by human breast cancer cells *in vitro*. Nature 1978;276: 726–8.

45. Sanchez-Sweatman OH, Orr FW, Singh G. Human metastatic prostate PC3 cell lines degrade bone using matrix metalloproteinases. Invasion Metastasis 1998; 18:297–305.

46. Stewart AF, Vignery A, Silverglate A, et al. Quantitative bone histomorphometry in humoral hypercalcemia of malignancy: uncoupling of bone cell activity. J Clin Endocrinol Metab 1982;55:219–27.

47. Sanchez Y, Bachant J, Wang H, et al. Control of the DNA damage checkpoint by Chk1 and Rad53 protein kinases through distinct mechanisms. Science 1999; 286:1166–71.

48. Mundy CR, Altman AJ, Gondek MD, Bandelin JG. Direct resorption of bone by human monocytes. Science 1977;196:1109–11.

49. Hall CL, Bafico A, Dai J, Aaronson SA, Keller ET. Prostate cancer cells promote osteoblastic bone metastases through Wnts. Cancer Res 2005;65:7554–60.

KAREN M. BUSSARD
Pathobiology Ph.D. Candidate
2137 North Oak Lane
State College, PA 16803
Cell: (717) 512-3813
Work: (814) 863-2434
kmb337@psu.edu

EDUCATION

The Pennsylvania State University, University Park, PA
Ph.D. in Pathobiology Date expected: May 2009
Ph.D. G.P.A. 3.95
Ph.D. thesis presently entitled "The Role of Osteoblast-Derived Inflammatory Cytokines in Bone Metastatic Breast Cancer"

The Pennsylvania State University, Hershey, PA
M.S. in Biomedical Engineering 2000-2002
Master's thesis entitled "Interactions of Model Biomaterials and Enzymes in Contact Activation of the Blood Plasma Coagulation Cascade"

Fairleigh Dickinson University, Madison, NJ
B.S. in Biology / minor in Chemistry 1995-1999
Honor's thesis entitled "Sports Injuries: How They Occur, Methods of Treatment, and Ways of Prevention"

WORK EXPERIENCE

Graduate Research Assistant 8/2004-present
The Pennsylvania State University, University Park, Pennsylvania
Advisor: Andrea M. Mastro, Ph.D., Professor of Microbiology and Cell Biology
- Investigate the influence of osteoblast-dervied inflammatory cytokines on metastatic breast cancer cells.
- Study and quantify the trafficking of breast cancer cells throughout long bones.
- Develop and perform protocols and analysis.
- Supervise, educate, and orient students in performance of protocols.

Research Support Associate/Graduate Research Assistant 8/2000 – 8/2004
The Pennsylvania State University, College of Medicine, Hershey, Pennsylvania
Advisor: Christopher A. Siedlecki, Ph.D,. Assistant Professor of Surgery and Bioengineering
- Study adhesion of blood coagulation factors to biomaterials with Atomic Force Microscope.
- Investigate the clotting mechanisms of human plasma in response to biomaterials.
- Analyze bovine blood of Left Ventricular Assist Device and Total Artificial Heart recipient research calves with the Thromboelastograph Hemostasis Analyzer (TEG).
- Develop and perform protocols and analysis.
- Supervise, educate, and orient assistant in performance of protocols.

Laboratory Technician II 10/1999 – 8/2000
University of Maryland Medical System, Baltimore, Maryland

- Blood Bank Technician assisting Medical Technologists in their work.
- Issue and perform ABO checks on blood products, receive, record, and sort blood specimens.
- Assist physicians in clinical decision making on product administration.
- Irradiate and thaw blood products.
- Cancer Center Platelet Laboratory Technician assisting physicians in clinical decision making of product administration and providing patients with platelets.

Laboratory Technician 10/1997 – 5/1999
Severn Trent Laboratories, Whippany, New Jersey

- Inorganics Laboratory Technician testing samples for Biochemical Oxygen Demand (BOD), Phenol distillation and reading, Alkalinity, Toxicity Characteristic Leaching Procedure (TCLP), ZHE tumbling and leaching, Total Suspended Solids (TSS), Total Dissolved Solids (TDS), Total Solids (TS), Reactivity, Cyanide, Specific Gravity, and Ignitability.
- Made reagents necessary for and calibrated instruments used for each test.

PROFESSIONAL MEMBERSHIPS

2002-2003	Society for Biomaterials
2003	American Society for Artificial Internal Organs
2005-present	Sigma Xi, The Scientific Research Society
2005-present	American Association for Cancer Research
2005-present	Women in Cancer Research (WICR)

PUBLICATIONS

2001 Siedlecki, CA, **Bussard, KM**, Vogler, EA. "FXII interactions with biomaterial surfaces." American Society for Artificial Internal Organs Journal. 47: (2), 170.

2005 Zhuo, R, Miller, R, **Bussard, KM**, Siedlecki, CA, Vogler, EA. "Procoagulant Stimulus Processing by the Intrinsic Pathway of Blood Plasma Coagulation." Biomaterials. 26: (16), 2965.

2005 Guo, Z, **Bussard, KM**, Chatterjee, K, Miller, R, Vogler, EA, Siedlecki, CA. "Mathematical Modeling of Material- Induced Blood Plasma Coagulation." Biomaterials. 27: (5), 796.

2006 Phadke, PA, Mercer, RR, Harms JF, Jia, Y, Kappes, JC, Frost, AR, Jewell, JL, **Bussard, KM,** Nelson, S, Moore, C, Gay, CV, Mastro, AM, Welch, DR. "Kinetics of Metastatic Breast Cancer Cell Trafficking in Bone." Clinical Cancer Research. 12: (5) 1431.

2007 Kinder, M, Chislock, EM, **Bussard, KM**, Shuman, LA, Mastro, AM. Metastatic Breast Cancer Induces an Osteoblast Inflammatory Response. Submitted.

ORAL PRESENTATIONS

2006 **Bussard, KM,** Phadke, PA, Mercer, RR, Harms JF, Jia, Y, Kappes, JC, Frost, AR, Jewell, JL, Nelson, S, Moore, C, Gay, CV, Mastro, AM, Welch, DR. "Kinetics of Metastatic Breast

Cancer Cell Trafficking in Bone." Presented at the American Association for Cancer Research Annual Meeting's Tumor Biology Minisymposium, April 1-5, 2006.

POSTER PRESENTATIONS

2002 **Bussard, KM**, Vogler, EA, Siedlecki, CA. "Effective Production of FXIIa and Thrombin by Model Biomaterials." Proceedings of the IEEE 28th Annual Northeast Bioengineering Conference, 02CH37342, April 20-21, 2002

2002 **Bussard, KM**, Vogler, EA, Siedlecki, CA. "Effective Enzyme Production of FXIIa and Thrombin by Model Biomaterials." Transactions of the 28th Annual Society for Biomaterials Conference, Volume XXV, April 24-27, 2002.

2003 **Bussard, KM**, Trivedi, SH, Vogler, EA, Siedlecki, CA. "Surface Acceleration of Blood Plasma Coagulation." Transactions of the 29th Annual Society for Biomaterials Conference, Volume XXVI, April 30-May 3, 2003.

2003 **Bussard, KM**, Zapanta, CM, Rosenberg, G, Pae, WE, Siedlecki, CA. "Thromboelastograph Evaluation of Bovine Blood." American Society for Artificial Internal Organs Journal 49: (2) 222. Presented at the Annual ASAIO-ISAO Joint Conference, June 19-21, 2003.

2005 **Bussard, KM,** Shuman, LS, Mercer, RR, Phadke, PA, Nelson, SM, Jewell, JL, Chislock, EM, Kinder, M, Welch, DR, Gay, CV, Mastro, AM. "The Interaction of Metastatic Breast Cancer Cells with Osteoblasts." Presented at the CrossOver 2005 Meeting sponsored by The Huck Institutes of The Life Sciences and The Materials Research Institute, The Pennsylvania State University, October 13-14, 2005.

2006 **Bussard, KM,** Chislock, EM, Kinder, M, Gay, CV, Mastro, AM. "A Classic Set of Osteoblast-Derived Inflammatory Cytokines is Produced in Response to Bone Metastatic Breast Cancer." The 11 th International Congress of the Metastasis Research Society, Tokushima, Japan, September 3-6, 2006.

2007 **Bussard, KM**, Mastro, AM. "Osteoblast-derived Inflammatory Cytokines are Produced in Response to Human Metastatic Breast Cancer Cells." The 100th Annual American Association for Cancer Research Annual Meeting, Los Angeles, CA, April 14-18, 2007. Proceedings of the 97th Annual Meeting for American Association for Cancer Research.

AWARDS AND HONORS

- American Association for Cancer Research – Women in Cancer Research Brigid G. Leventhal Scholar Award in Cancer Research: 2006.
- Department of Defense Predoctoral Traineeship Award in Breast Cancer (Fellowship): 2006-2009.
- Sigma Xi Grants-in-Aid of Research: 2005-2006.
- The Pennsylvania Space Grant Consortium NASA Space Grant Fellowship: 2005-2007.
- Chancellor's List Publication: Inaugural Edition (2005), 2006.
- Honorable Mention for Student Travel and Professional Development Award, Society for Biomaterials: 2002.

- FDU Outstanding Academic Excellence Award in Biology: May 1999.
- FDU James A. Griffo Award for Academic Excellence and Athletic Achievement during college career: May 1999.
- FDU University Honors Program: 1995-1999 (Senior thesis entitled “Sports Injuries: How they occur, Methods of Treatment, and Ways of Prevention” presented April 30, 1999).
- FDU Presidential Scholar (Full Academic Tuition Scholarship): 1995-1999.
- Member: Phi Zeta Kappa (FDU Junior Honor Society, GPA 3.5+).
- Member: Phi Omega Epsilon (FDU Senior Honor Society, GPA 3.5+).
- Who’s Who of Students in American Colleges and Universities Publication: 1995-1999.
- The National Dean’s List Publication: 1995-1999.